AD-A251 832

MENTATION PAGE

Form Approved
OMB No. 0704-0188

1. AGENCY USE ONLY (Leave blank)	2. REPORT DATE	3. REPORT TYPE AND DATES COVERED
		Final Report 01 Jun 91-29 Feb 92

4. TITLE AND SUBTITLE
A coherent x ray source using transition radiation

5. FUNDING NUMBERS
F49620-91-C-0041

6. AUTHOR(S)
M. A. Piestrup, Qiang Li, A.H. Hoe & B.G. Boyers

AFOSR-TR- 92 [illegible]8

7. PERFORMING ORGANIZATION NAME(S) AND ADDRESS(ES)
Adelphi Technology Inc
2181 Park Blvd
Palo Alto, CA 94306

8. PERFORMING ORGANIZATION REPORT NUMBER

9. SPONSORING / MONITORING AGENCY NAME(S) AND ADDRESS(ES)
AFOSR/NE, SCHLOSSBERG
Bldg 410
Bolling AFB DC 20332-6448

10. SPONSORING / MONITORING AGENCY REPORT NUMBER
3005/A1

DTIC
ELECTE
JUN 18 1992
S A D

11. SUPPLEMENTARY NOTES

12a. DISTRIBUTION / AVAILABILITY STATEMENT
Original contains color plates: All DTIC reproductions will be in black and white

UNLIMITED

This document has been approved for public release and sale; its distribution is unlimited.

12b. DISTRIBUTION CODE

13. ABSTRACT *(Maximum 200 words)*

The major goal of this work was to establish the commercial feasibility of a compact, quasimonochromatic, collimated x-ray source. We analyzed x ray emission from foil stacks with uniform foil thickness and spacing, known as coherent transition radiation. We found that compared with ordinary, or incoherent radiators, these sources can have reduced angles of emission as well as increased brightness. In addition, the radiation pattern is confined to a narrower range of angles, allowing for more efficient focusing using grazing incidence optics, and resulting in even higher x-ray intensities.

Our findings were based on both theoretical and experimental work. We measured x rays in the 1-5 keV energy range, generated by a coherent transition radiator composed of 35 mylar foils. We were also able to focus transition radiation using simple cylindrical optics. Submillimeter spot sizes have been obtained with incoherent radiators. The effects of emittance on the electron beam as well as errors in the foils spacing were studied using computer simulation we developed. The brightness of the source was found to compare favorable with synchrotron radiators.

14. SUBJECT TERMS			15. NUMBER OF PAGES
			16. PRICE CODE
17. SECURITY CLASSIFICATION OF REPORT	18. SECURITY CLASSIFICATION OF THIS PAGE	19. SECURITY CLASSIFICATION OF ABSTRACT	20. LIMITATION OF ABSTRACT

FINAL REPORT

The Department of the Air Force
Air Force Office of Scientific Research
Small Business Innovative Reseach Program
Phase I contract,
F49620-91-C-0041, DEF
July 1991 to Feb. 1992.

A COHERENT X RAY SOURCE USING TRANSITION RADIATION

Principal Investigator: M. A. Piestrup
Associate Investigators: Qiang Li, A. H. Ho and D. G. Boyers

Adelphi Technology Inc.,
2181 Park Blvd.,
Palo Alto, California 94306

FINAL REPORT

U.S. DEPARTMENT OF DEFENSE

SMALL BUSINESS INNOVATION RESEARCH PROGRAM

PHASE 1

PROJECT SUMMARY

Topic No. AF91-196 Military Department/Agency USAF .

Name and Address of Proposing Small Business Firm

Adelphi Technology, Inc.
2181 Park Blvd.
Palo Alto, CA 94306

Name and Title of Principal Investigator

Dr. Melvin A. Piestrup, President

Title Proposed by Small Business Firm

A Coherer X-ray Source Using Transition Radiation

Technical Abstract (Limit your abstract to 200 words with no classified or proprietary information/data.)

The major goal of this work was to establish the commercial feasibility of a compact, quasimonochromatic, collimated x-ray source. We analyzed x ray emission from foil stacks with uniform foil thickness and spacing, known as coherent transition radiation. We found that compared with ordinary, or incoherent radiators, these sources can have reduced angles of emission as well as increased brightness. In addition, the radiation pattern is confined to a narrower range of angles, allowing for more efficient focusing using grazing incidence optics, and resulting in even higher x-ray intensities.

Our findings were based on both theoretical and experimental work. We measured x rays in the 1-5 keV energy range, generated by a coherent transition radiator composed of 35 mylar foils. We were also able to focus transition radiation using simple cylindrical optics. Submillimeter spot sizes have been obtained with incoherent radiators. The effects of emittance on the electron beam as well as errors in the foils spacing were studied using computer simulation we developed. The brightness of the source was found to compare favorably with synchrotron radiators.

Anticipated Benefits/Potential Commercial Applications of the Research or Development

Among the many practical applications of a quasimonochromatic, high brightness x-ray source are: study of biological materials using Laue diffraction, x-ray lithography for the production of integrated circuits, and pulsed-x-ray generation for radiation damage studies. Coherent transition radiation can utilize the inherent pulsed structure of many accelerators to produce a high brightness pulsed x-ray source which can be used to study many transient effects in solids and biological materials. Coherent transition radiators can be added to existing accelerators or be designed with microtrons of moderate electron beam energy to give a compact x-ray source of relatively moderate cost as compared to synchrotron emitters.

List a maximum of 8 Key Words that describe the Project.

Pulsed x ray, transition radiation, x ray, lithography, synchrotron, accelerator

PROJECT SUMMARY

The major goal of this work was to establish the commercial feasibility of a compact, quasimonochromatic, collimated x-ray source. We analyzed x ray emission from foil stacks with uniform foil thickness and spacing, known as coherent transition radiation. We found that compared with ordinary, or incoherent radiators, these sources can have reduced angles of emission as well as increased brightness. In addition, the radiation pattern is confined to a narrower range of angles, allowing for more efficient focusing using grazing incidence optics, and resulting in even higher x-ray intensities.

Our findings were based on both theoretical and experimental work. We measured x rays in the 1-5 keV energy range, generated by a coherent transition radiator composed of 35 mylar foils. We were also able to focus transition radiation using simple cylindrical optics. Submillimeter spot sizes have been obtained with incoherent radiators. The effects of emittance on the electron beam as well as errors in the foils spacing were studied using computer simulation we developed. The brightness of the source was found to compare favorably with synchrotron radiators.

We found that the bandwidth of the coherent radiators can be narrowed by designing the radiator to emit near the foil materials photoabsorption edge. Bandwidths of 30 to 60 % are possible across the x-ray region of the spectrum. Under another contract, this effect using incoherent radiators has been observed from 1.5 keV using aluminum foils to 20 keV using molybdenum foils.

Among the many practical applications of a quasimonochromatic, high brightness x-ray source are: study of biological materials using Laue diffraction, x-ray lithography for the production of integrated circuits, and pulsed-x-ray generation for radiation damage studies. Coherent transition radiation can utilize the inherent pulsed structure of many accelerators to produce a high brightness pulsed x-ray source which can be used to study many transient effects in solids and biological materials. Coherent transition radiators can be added to existing accelerators or be designed with microtrons of moderate electron beam energy to give a compact x-ray source of relatively moderate cost as compared to synchrotron emitters.

TABLE OF CONTENTS

1. INTRODUCTION

High power x-ray sources are being applied to such varied uses as high resolution medical imaging, x-ray microscopy, and microlithography. The development of these technologies will be facilitated by the availability of a relatively inexpensive, high brightness x-ray source. In an extended series of experiments at the Lawrence Livermore National Laboratory (LLNL), Naval Postgraduate School (NPS), and Saskatchewan Accelerator Laboratory (SAL) linear accelerators, we have studied the feasibility of using transition radiation (TR) as such a source.[1-5] Our experiments have measured the spectral and spatial characteristics of TR for a wide variety of experimental conditions,[6-23] and in most cases have shown excellent agreement with theory. The experimental results have shown high photon-production efficiencies as well as coherence, quasimonochromaticity, and the ability to focus TR using grazing incidence optics.

A major benefit of such a source is that it requires a relatively low electron beam energy as compared to synchrotron radiation sources, and can be generated by room-size accelerators such as microtrons or pelitrons. Calculations and experiments[8,19] show that transition radiation sources in the soft x-ray region of 0.1-2.0 keV can be generated using electron beam energies of less than 20 MeV. In comparison, synchrotron radiation requires much higher electron beam energies to produce similar x-ray energies.

A problem with transition radiation, however, is that the x-ray emission is found in an annular ring whose angular divergence is sufficiently large that the resulting spot size is large compared to typical synchrotron radiation beam sizes. This is especially true for transition radiation generated by moderate to low energy electrons (< 50 MeV). The result is reduced x-ray intensities.

In our phase I work, we analyzed transition radiation from foil stacks with uniform foil thickness and spacing, known as coherent or resonant transition radiation (RTR). We found that compared with ordinary, or incoherent radiators, these sources can have reduced angles of emission as well as increased brightness. In addition, the radiation pattern is confined to a narrower range of angles, allowing for more efficient focusing using grazing incidence optics, and resulting in even higher x-ray intensities.

Our findings were based on both theoretical and experimental work. We measured x rays in the 1-5 keV energy range, generated by a coherent transition radiator composed of 35 mylar foils. We were also able (under a phase II NSF-SBIR project) to focus transition radiation using simple cylindrical optics. The effects of emittance on the electron beam as well as errors in the foils spacing were studied using computer simulations we developed. The brightness of the source was found to compare favorably with synchrotron radiators.

Another problem with TR is that the radiation is in general broadband. In our phase I work we were able to demonstrate, both theoretically and experimentally, that by proper selection of the radia-

tor foil thickness, number, and meterial, the bandwidth can be designed to vary anywhere between 20-60%.

When comparing x-ray sources, one simple unit of comparison is the production efficiency measured in terms of photons generated per incident electron. A TR source driven by a 100 MeV electron beam can generate more than 0.1 photons/electron-keV in the soft x-ray region. This efficiency is many orders of magnitude greater than what can be achieved by conventional electron-driven bremsstrahlung of characteristic-line sources and is two to three orders of magnitude more efficient than synchrotron sources driven by electrons with energies in the GeV range.

In the remainder of this report, we will describe in more detail how the brightness of TR can be increased by using interfoil phase coherence (RTR) as well as by focusing using grazing incidence optics (indeed the radiation pattern generated by RTR is particularly amenable to focusing using simple cylindrical optics). We will report on both theoretical and experimental work. Finally, we will compare RTR with synchrotron radiation sources.

2. DEGREE TO WHICH PHASE I OBJECTIVES HAVE BEEN MET

2.1 PHASE I TECHNICAL OBJECTIVES

The specific objectives of phase I of this research are:

GOAL I. Demonstrate that coherent transition radiation can be used to increase the intensity and reduce the angle of emission from the incoherent case. Include the effects of scattering and higher mode generation.

GOAL II. Reduce the bandwidth of the x-ray source by either photoabsorption edge truncation or by using the resonance effect. Use antenna-array theory to design radiators.

GOAL III. Design a compact x-ray source by minimizing the size of the electron-beam source. Determine the minimum electron-beam energy to obtain resonance transition radiation.

2.2. BRIEF SUMMARY OF PHASE I RESULTS

A list of our phase I goals and a brief summary of our results is as follows:

GOAL I. Demonstrate that coherent transition radiation can be used to increase the intensity and reduce the angle of emission from the incoherent case. Include the effects of scattering and higher mode generation.

We compared coherent and incoherent transition radiators both theoretically and experimentally. We found that the most obvious manifestation of coherence was the alteration of the spatial emission pattern. There is also an alteration of the emission spectrum in the form of dispersion and narrowing of the bandwidth of the x-ray spectrum. The spatial alteration of the emission pattern can be used to increase the x-ray flux by passing through cylindrical optics. The dispersion of the x-rays can be utilized to narrow the focused spectrum of the x rays. Using the grazing incidence optics and resonance TR a bright source of quasimonochromatic x rays is produced. Under phase II, we will utilize a exist-

ing electron beam, x-ray optical alignment system and resonance transition radiators to produce a bright, focused x-ray source.

We analyzed the the effects on the x-ray spatial distribution from elastic scattering of the electrons and higher mode generation. For low density foils such as beryllium and aluminum, scattering was of little significance. Scattering must be taken into account for higher density foils such as zinc and molybdenum foils.

We also studied the effect of the electron-beam emittance or the x-ray spatial distribution. A computer simulation was modified to display the spatial distribution of the emission from an ideal resonance emitter.

In addition we compared coherent and incoherent TR with synchrotron radiation from single bend magnets such as those found at the Stanford Synchrotron Radiation Laboratory (SSRL). We found that the number of photons/electron from a resonance emitter can be greater by a factor of 10 or more than that obtained from a synchrotron emitter. If the accelerator source is pulsed (as in most linacs), the brightness of RTR can be close to that of wigglers.

GOAL II. Reduce the bandwidth of the x-ray source by either photoabsorption edge truncation or by using the resonance effect. Use antenna-array theory to design radiators.

We studied the effect of foil spacing (resonance) and foil x-ray transmission on the the bandwidth of the x-ray spectrum. We found that by far the most effective method for achieving bandwidth narrowing was by using absorption of the foil to narrow the spectrum. By designing the transition radiator to emit x rays at the foil materials K-shell photoabsorption edge, the x-ray spectrum is narrowed. The resultant source is quasimonochromatic (40 to 50% bandwidth) and does not depend upon the resonance effect. Previously, under the DOE-SBIR program we observed such quasimonochromatic radiation from Al, Mg and Ti foils at soft x ray energies (1 to 5 keV). In Nov. 1991, we also observed bandwidth narrowing using Zn and Mo radiators at 9 and 20 keV. These were incoherent radiators and not designed to achieve phase coherence between foils.

We developed a computer simulation which utilized nouniform spacing of the foils. The program can be used to predict both the spatial and spectral distribution of the x-ray emission. We found that small variations in the foil spacings on the order of microns did not charge the spatial distribution of RTR significantly.

GOAL III. Design a compact x-ray source by minimizing the size of the electron-beam source. Determine the minimum electron-beam energy to obtain resonance transition radiation.

The minimum electron energy required for RTR was determined for various bandwidths and for various resonance emitters. The desired electron-beam energy will depend upon a number of factors including the desired application for the x rays. For best economy, a single klystron linac or micro-

tron producing electrons of 50 MeV or larger would be used. We have designed a RTR source utilizing known linac and microtron sources. Single-klystron microtrons can produce 50 to 150 MeV electrons. Such accelerators permit a soft to hard x-ray source to be constructed for under 5 million dollars.

In this report we present the footprint of a known commercial microtron and the positioning of a number of stations for commercial x ray lithography.

2.2. MAJOR BREAKTHROUGHS

The major breakthroughs in knowledge acquired under this phase I AFOSR contract are as follows:

1. We found that RTR with cylindrical optics will produce a high intensity, focused x-ray beam of less than 1 mm in diameter. We have shown this to be the case both experimentally and theoretically. The intensity of the focused coherent radiation is larger than focused incoherent TR by an order of magnitude.

2. We demonstrated coherence from a RTR stack with a large number of foils. Previously, the maximum number of foils used was 8; we have now extended this to 35 foils. This is important in order to increase the total x-ray flux. In addition we have extended RTR from 1 keV photons to 5 keV.

3. We have found that the major alteration of the RTR spatial distribution is due to the finite electron-beam emittance and not random variation in foil spacing. Moderate energy (50 to 75 MeV) electron beams with good quality emittance will produce a better x-ray annulus for focusing.

3. RESONANCE TRANSITION RADIATION

3.1. INTRODUCTION

TR occurs when a moving charged particle encounters a sudden change in dielectric constant, such as occurs at an interface between two media (or between a vacuum and a medium) [1-3,13-15] The amount of radiation produced is small from a single interface; however, if a number of foils are placed in sequence the x-rays produced at each foil can add linearly. If the foil spacing is accurate enough there can be phase addition between foils as well as between the front and back surfaces of single foils. Constructive interference can occur for certain photon energies and in certain directions. Note that the interference can occur for a single photon, just as in the case of a diffraction grating; that is, the interference is of a quantum mechanical nature.

3.2. SPECTRAL AND SPATIAL DISTRIBUTIONS

Ordinarily, a particle which is moving with constant velocity does not radiate unless the particle velocity equals the phase velocity of the emitted wave along the direction of particle motion, as in the case of Cherenkov radiation. However, if the interaction length is limited, or equivalently, if the die-

lectric constant is suddenly changed, as at the interface between two media, then velocity matching is not necessary. The minimum distance over which an electromagnetic wave and a charged particle can exchange energy is called the formation length, and is given by[14]

$$z_i\ (i = 1, 2) = \frac{2c}{\omega\left[1 - \beta\sqrt{\epsilon_i - \sin^2\theta}\right]} \simeq \frac{4\lambda\beta}{\left[\frac{1}{\gamma}\right]^2 + \theta^2 + \left[\frac{\omega_i}{\omega}\right]^2} \qquad (1)$$

where $\gamma = (1 - \beta^2)^{-1/2}$, $\epsilon_i = 1 - (\omega_i/\omega)^2$ are the permittivities of the two media, ω_i are their respective plasma frequencies, $\beta = v/c$, v is the speed of the electron, c the speed of light, $\lambda = c/\omega$ and θ is the angle of emission. Thus, there is emission at the interface if the material thickness on both sides of the interface is on the order of z_1 and z_2 or greater.

Emission can also occur for multiple interfaces such as between foils whose thicknesses are on the order of z_2 interspersed in a vacuum with separation on the order of z_1. These interfaces can be randomly spaced, as in foam plastic, or periodically spaced. As shown diagrammatically in Fig. 3.1, the x rays are emitted conically in an annulus whose apex angle of emission is $\theta_S \simeq 1/\gamma$ when there is no constructive phase addition between foils.

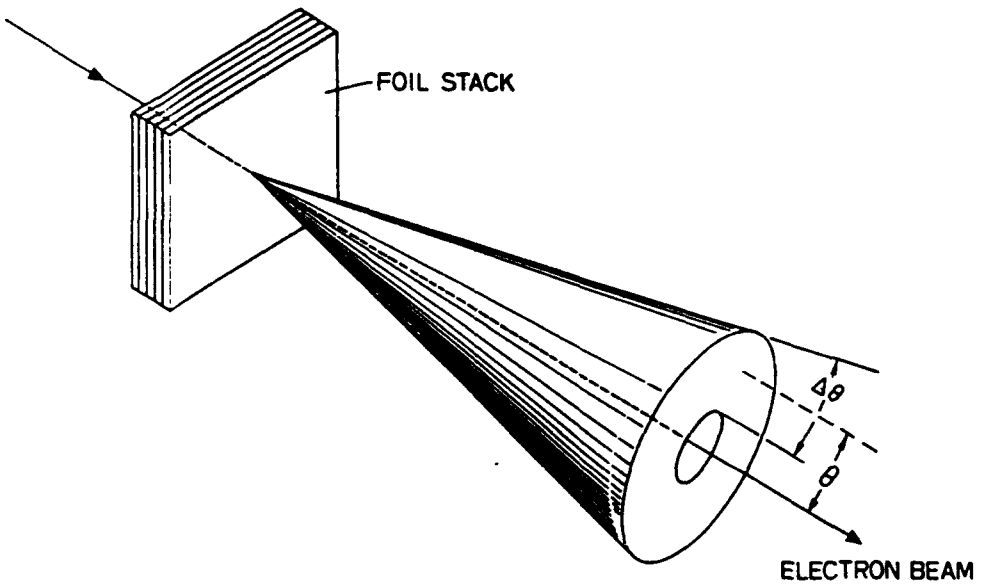

Fig. 3.1. A schematic diagram of the cone of emission produced by transition radiation showing the peak emission angle and range of emission angles $\Delta\theta$. The coherent x-rays are emitted in a small forward cone whose apex angle is dependent upon the foil spacing, foil thickness, foil material, and charged-particle energy.

The differential cross section for transition radiation production per photon energy interval per solid angle is given by an expression of the form[4,14]

$$\frac{d^2N(\omega)}{d\omega d\Omega} = F_1 \cdot F_2 \cdot F_3, \tag{2}$$

where $N(\omega)$ is the number of photons and ω is their radial frequency.

The first factor F_1 is the contribution from a single interface and is given by[14]

$$F_1 = \frac{\alpha\omega \sin^2 \theta}{16\pi^2 c^2} \cdot (z_1 - z_2)^2, \tag{3}$$

where α is the fine-structure constant.

There is an angle that maximizes the radiation F_1 from a single interface. For most cases $\theta^2 \ll 1$, $\epsilon_i \simeq 1$, and $\beta \simeq 1$, and so this is[14]

$$\theta^2_S = \frac{1}{3}\{-(\delta_1 + \delta_2) + [(\delta_1 + \delta_2)^2 + 12\delta_1\delta_2]^{1/2}\} \tag{4a}$$

where $\delta_i = \frac{1}{2\gamma^2} + \frac{\omega^2_i}{2\omega^2}$.

A first order approximation is:

$$\theta_S \simeq \sqrt{\frac{1}{\gamma^2} + \left[\frac{\omega_1}{\omega}\right]^2} \tag{4b}$$

where ω_1 is the plasma frequency of the interfoil gas. If there is a vacuum between the foils, then $\omega_1 = 0$ and $\theta_S \simeq 1/\gamma$. There may be considerable intensity, however, up to the angle:[14]

$$\theta_m \simeq \sqrt{\frac{1}{\gamma^2} + \left[\frac{\omega_2}{\omega}\right]^2} \tag{5}$$

where ω_2 is the plasma frequency for the foils.

The second factor F_2 accounts for the coherent superposition of radiation from the two surfaces of a single foil. If the incoherent effects of electron collisions within the foil and the photon attenuation through the foil are ignored, F_2 assumes the familiar two-source interference pattern

$$F_2 = 4 \sin^2\left[\frac{\ell_2}{z_2}\right], \tag{6}$$

where ℓ_2 is the thickness of the foil. The factor-of-four increase in peak intensity is the most striking manifestation of the two-surface constructive interference.

The third factor F_3 describes the summation of contributions from each foil in the stack. Again, there is a superposition of M (the number of foils) coherent sources. In its simplest form,

$$F_3 = \frac{\sin^2 MX}{\sin^2 X}, \tag{7}$$

where $X = \left[\frac{\ell_1}{z_1}\right] + \left[\frac{\ell_2}{z_2}\right]$.

In the case of a periodic medium, a $r\pi$-phase slippage is the condition for constructive interference or resonance between foil interfaces. If the foil thicknesses are not z_1 and z_2, the maximum

energy exchange and resonance occur when:

$$X = \frac{\ell_1}{z_1} + \frac{\ell_2}{z_2} = r\pi \tag{8a}$$

$$\frac{\ell_2}{z_2} = (m - 1/2)\pi \tag{8b}$$

where r and m are positive integers.

Using these values for ℓ_1 and ℓ_2, Eq. (2) becomes

$$\frac{d^2N}{d\Omega d\omega} = 4M^2F_1 \tag{9}$$

Eqs. (8a) and (8b) are the coherence conditions, i.e., the requirements for in-phase addition of the radiation from all interfaces. To minimize photon absorption and electron scattering, ℓ_1 should be as small as possible, which means choosing r = m = 1. For those values,

$$\ell_{1,2} = \left[\frac{\pi}{2}\right] z_{1,2}. \tag{10}$$

Substituting into Eq. (8a) expressions for z_1 and z_2 and solving for cos θ, we obtain:

$$\cos\theta_r = \frac{\ell_1 + \ell_2}{\ell_1\sqrt{\epsilon_1} + \ell_2\sqrt{\epsilon_2}}\left[\frac{1}{\beta} - \frac{r\lambda}{\ell_1 + \ell_2}\right] \tag{11}$$

This is the angle at which phase matching between waves can occur at each interface (Fig. 3.2).[3] For small angles, Eq. (11) can be written as

$$\theta_r^2 = \frac{2r\lambda}{\ell} - \frac{1}{\gamma^2} - \left[\frac{\omega_0}{\omega}\right]^2 \tag{12}$$

where $\omega_0^2 = (\omega^2_1\ell_1 + \omega^2_2\ell_2)/(\ell_1 + \ell_2)$ and $\ell = \ell_1 + \ell_2$.

From (11) and (12) we see that the angle of emission is determined by the foil thickness and the energy of the emitting particle. We note that θ_r can be greater than $1/\gamma$, which would allow the measurement of extremely relativistic electrons. Unlike the single interface angle of emission, θ_r increases with electron-beam energy.

If the cumulative photon attenuation through the successive foils is included, then F_3 takes the form[4,16]

$$F_3 = \frac{1 + \exp(-M\sigma) - 2\exp\left[-\frac{M\sigma}{2}\right]\cos(2MX)}{1 + \exp(-\sigma) - 2\exp\left[-\frac{\sigma}{2}\right]\cos(2X)} \tag{13}$$

where $\sigma = \mu_1\ell_1 + \mu_2\ell_2$ and μ_i are the x-ray-absorption coefficients.

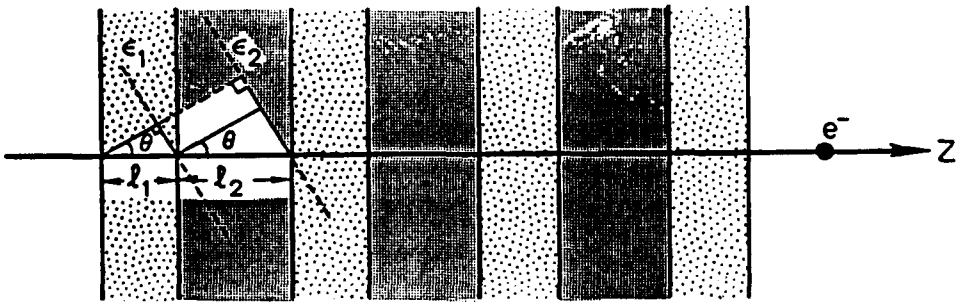

Fig. 3.2. Resonance transition radiation from a periodic medium with uniform spacing. If the phase velocity of the emitted radiation along the z-direction slips out of phase by $2\pi r$ rad (r is an integer) for each foil pair interface, the radiation adds in phase and the intensity varies as square of the number of foils.

Two kinds of simulation routines were performed which calculate angular distributions and photon-energy spectrums. Integrating Eq. (2) over bandwidth of the detector, one obtains the angular distribution of the photons. Integrating over the angular scan of the detector, one obtains the photon energy spectrum. Integrations were done by the Simpson-rule method.

3.3. THE FUNDAMENTAL RESONANCE MODE

As can be seen from Eqns. (11) and (12), a large number of r values or modes is possible. The resulting angular distribution from all these modes depends upon the number of foils and frequency band of emission. In some cases the distribution breaks up into a multiple-lobe pattern.[9,10] However, we can make the r = 1 mode dominate by choosing r = m = 1, and by limiting the angle of peak emission to $0 < \theta_r < \theta_m$. We calculate ℓ_1 and ℓ_2 by substituting the desired θ and ω into Eq. (10). Knowing the absorption of the foil material, we then calculate the number of foils from $M < 2/\mu\ell_2$. The mode thus selected is dominated by a single peak characteristic of the r = m = 1 mode as shown in Fig. 3.3. As the number of foils is increased, the mode becomes more pronounced and peaked. The shape of the mode produced under these conditions is similar for other x-ray energies and has a universal shape when radiation is optimized near the angle of peak emission ($\theta_r = \theta_s \simeq 1/\gamma$ for the single-interface term (eq (3)). The mode has a characteristic slow rise to the peak with a sudden fall-off after θ_r. Fig. 3.3 shows the calculated transition-radiation angular distribution for 300-MeV electrons for varying numbers of mylar foils. As the number of foils increases, the angular peak becomes more pronounced, narrowing the thickness of the x-ray annulus.

The desired frequency for resonance can be chosen between the high end of the spectrum where the cutoff frequency is approximately given by $\omega_c = \gamma\omega_p$ and the low end of the spectrum where absorption is so dominant that only a small number of foils can be used. Designing the radiator to

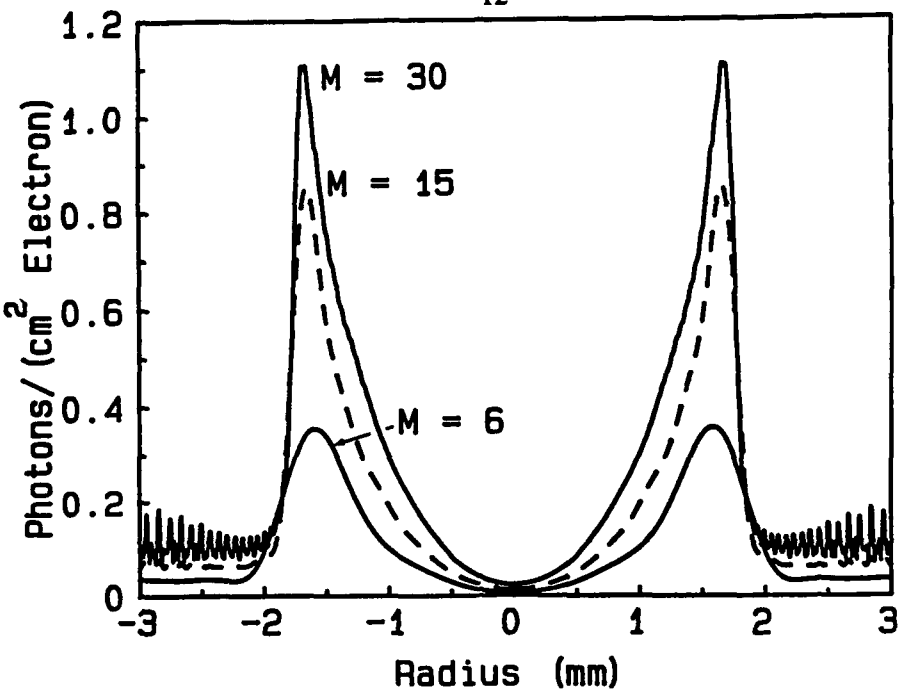

Fig. 3.3. The calculated spatial photon density as a function of radial distance from the axis of the electron beam from three mylar-foil stacks with foil numbers of M = 6, 15, and 30. The stacks were all designed to have peak emission at $\theta_r \simeq 1/\gamma = 1.7$ mrad at 4 keV. The electron-beam energy is 300 MeV. The foil thickness and spacing for this design are $\ell_2 = 5.6$ μm and $\ell_1 = 16.4$ μm. The distance from the radiator to the detection plane is 1 m. As the number of foils increases, the peak of the annulus becomes more pronounced.

resonate at harder x-ray energies permits a large number of foils to be used.

We can design foil stacks to be resonant at any desired angle between $0 < \theta_r < \theta_m$. Incoherent radiation is confined to diverge at $1/\gamma$, independent of foil thickness and spacing. From Eq. 12 we see that the angle of emission, θ_r, of the resonance stack is determined by the foil thickness and the energy of the emitting electron. In Figs. 3.4, we show measured RTR spatial distributions where the angular divergence of the peak is (a) less than that of the incoherent TR and (b) greater than that of the incoherent TR. θ_r can be smaller than $1/\gamma$, which would allow the divergence of the x-rays to be minimized, thus facilitating the use of grazing angle optics to focus the x rays.

Plotting θ_r as a function of energy in Fig. 3.5, we see that the angle has a threshold value then rising with increasing energy reaching an asymptotic value. In contrast the angle of peak emission of the incoherent case decreases with increasing electron-beam energy, following Eq. (3.4a) (approximately as $\theta_s \simeq 1/\gamma$). Thus the functional dependence of the angle of peak emission for the two cases of randomly-spaced and periodically-spaced foils is markedly different. For example in our experiment described in Section 6, we compared the angle separation of the peaks of the annulus as a function of the electron-beam energy. This gave us conclusive evidence that we were observing coherence.

The approximate spatial width of the annulus can be determined by a simple calculation. Bor-

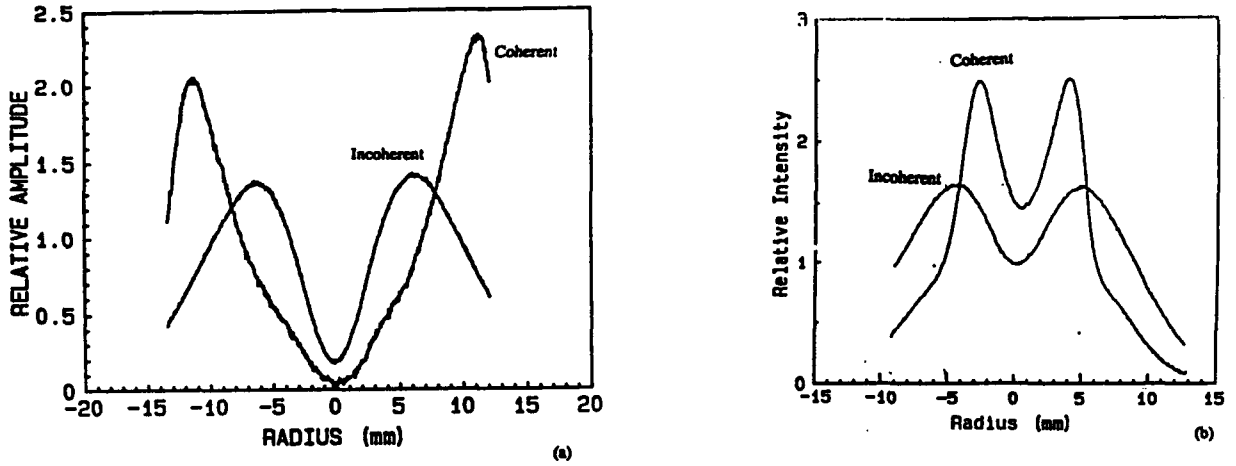

Fig. 3.4. The measured spatial distribution for the coherent and incoherent radiators. In (a) the resonance stack is designed to have its angle of peak emission greater than that of the incoherent radiator, while in (b) less than that of the incoherent radiator. The stacks both have the same foil thickness and number, but with different spacing (see ref. 19).

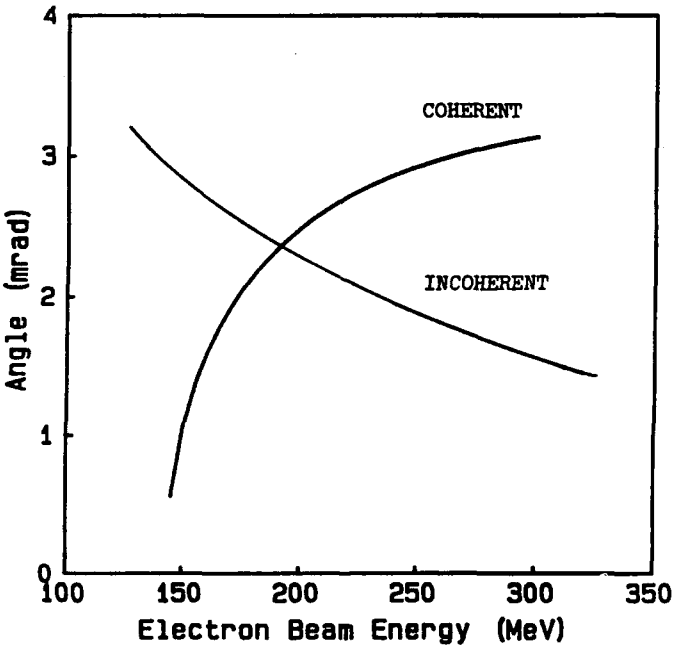

Fig. 3.5. The calculated angle of peak emission as a function of energy. The angle of peak emission increases with energy for RTR and decreases for incoherent TR. The foil stacks have identical foil number and thickness (ℓ_2 = 6.4 μm and M = 35) but different spacing (RTR: ℓ_1 = 30 μm; incoherent: ℓ_1 $\simeq$135 μm).

rowing from antenna theory, we can define the beamwidth to be the angular space between the first nulls on each side of the r = m = 1 peak. The location of the nulls can form F_3 given by Eq. (4.13). The null of F_3 occur when Sin MX=0, or $MX_n = \pi n$ (n is an integer), that is, when $\ell_1/Z_1 + \ell_2/Z_2 = n/M\pi$. Substitution of Z_1 and Z_2 from Eq. (4.1) yields for the null locations:

$$\mathrm{Cos}\theta_n = \frac{\ell_1 + \ell_2}{\ell_1\sqrt{\epsilon_1} + \ell_2\sqrt{\epsilon_2}}\left[\frac{1}{\beta} - \frac{n\lambda}{M}(\ell_1 + \ell_2)\right] \tag{14}$$

or:

$$\theta_n^2 = \frac{2n\lambda}{M\ell} - \frac{1}{\gamma^2} - \left[\frac{\omega_0}{\omega}\right]^2 \tag{15}$$

thus the angular beamwidth of the first first mode is:

$$\Delta\theta = [\theta_1 - \theta_2] \simeq 0.4\sqrt{\frac{\lambda}{M\ell}} \tag{16}$$

3.4. RANDOMIZING EFFECTS

For a correctly designed RTR stack, coherence can be destroyed by three processes: (1) variation in foil thickness and spacing, (2) finite electron-beam emittance and (3) elastic scattering in the foils. A somewhat counter-intuitive finding was that for realistic electron-beam and foil-stack parameters, the random variation in the foil spacing least affected the angular distribution. The three randomizing processes are discussed in the following three sections.

3.4.1. Nonuniform spacing

Random variation in the foil thicknesses and spacing can destroy coherency. Garibyan et al. have shown that if the variation in foil thicknesses and spacing satisfies the inequality[15,16]

$$2M\left[\frac{\Delta_1^2}{z_1^2} + \frac{\Delta_2^2}{z^2_2}\right] \ll 1 \tag{17}$$

where Δ_1 and Δ_2 are the standard deviations in foil dimensions, then it can be shown that for $M \gg 1$ and for the r = m = 1 case

$$\frac{\ell_1}{z_1} = \frac{\ell_2}{z_2} = \frac{\pi}{2} \tag{18}$$

then[16]

$$\frac{d^2N}{d\Omega d\omega} \simeq 4M^2\left[1 - \frac{4M}{3}\left[\frac{\Delta^2_1}{z^2_1} + \frac{\Delta^2_2}{z^2_2}\right]\right]\frac{d^2N_0}{d\Omega d\omega} \tag{19}$$

where $\ell_{1,2}$ are the mean spacing and thickness. Thus, when Eq. (19) is satisfied, the reduction in emission from the ideal coherent case resulting from variations in thickness is small. An upper bound on the standard deviation of the thickness and spacing would be approximately:

$$\Delta_1 < \frac{z_1}{\sqrt{2M}} \tag{20a}$$

$$\Delta_2 < \frac{z_2}{\sqrt{2M}} \tag{20b}$$

For example, in the case of the radiator used in our AFOSR experimental work, $\ell_1 = 30$ μm, $\ell_2 = 6.4$ μm, and M = 35, the upper bounds on the standard deviations are $\Delta_2 < 0.5$ μm and $\Delta_1 < 2.3$ μm. These are not unreasonable mechanical tolerances.

Under this AFOSR contract, we have further investigated the effect of foil spacing. We designed a simulation program (called NONUNI) in which we calculated both the spectral and spatial distributions for foil stacks whose foil spacing can be individually selected. Using this program, we simulated the spatial distribution for foil stacks whose average spacings had various standard deviations. Typical results from NONUNI are shown in Fig. 3.6 using the the mylar stack constructed for the SAL experiment. Fig. 3.6 shows that a the standard deviation of over 5 μm for a mean foil spacing of 30 μm can be tolerated without undue broadening of the x-ray annulus. Thus we are able to construct periodic structures whose parameter accuracies are on the order of infrared wavelengths and yet are "resonant" or coherent for soft x-ray wavelengths.

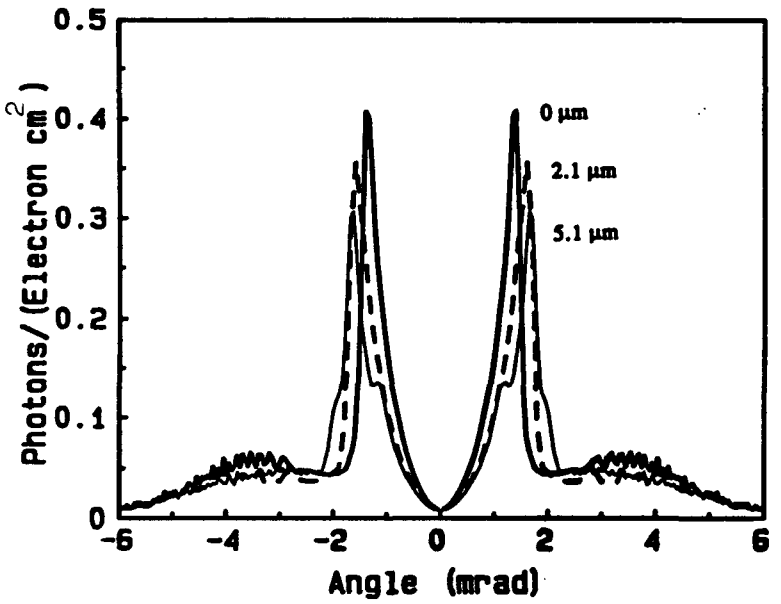

Fig. 3.6. The calculated angular distribution of the x-ray annulus as a function of angle for foil stacks which have an average foil spacing of $\ell_1 = 30$ μm with individual standard deviations of 0, 2.1 μm, and 5.1 μm. The electron-beam energy is 175 MeV. The mylar-foil thickness is assumed to be a constant $\ell_2 = 6.4$ μm and M = 35.

Note, if the distances ℓ_1 or ℓ_2 are completely random, or if the angular and spectral structure associated with Eq. (13) cannot be resolved by the experiment, then Eq. (13) must be averaged over X. This yields[4,14]

$$F_3 = \frac{1 - \exp(-M\sigma)}{\sigma} \tag{21}$$

and is termed incoherent TR.

3.4.2. Electron-beam emittance

We have written two programs to study the effect of electron-beam emittance on spatial distribution. One of these programs (REFLECT) can include a reflecting cylindrical optic. REFLECT is a Monte Carlo simulation which, given an electron-beam of given divergence and size, calculates individual x-ray beam trajectories from the transition radiator to the optic and, finally, to the detector.

A simpler program (EMIT) is used to calculate the effect of the electron-beam emittance on the spatial distribution. This program takes an input point-source photon distribution from our SIMUL2 program and convolves it with a radially Gaussian-distributed electron beam. The Gaussian is defined by a standard deviation, which is the quadratic sum of the electron-beam size and its divergence. We input the electron-beam diameter in mm, the electron-beam divergence in mrad, and the distance from the radiator to the detector. The output then gives the distribution of x-rays of a real source with finite size and divergence.

Using EMIT, we calculated the spatial distribution for an RTR stack to be constructed in phase II. The results are given in Fig. 3.7. The emittance of the SAL linac is case (b) in the figure. As we can see the peak has been reduced by a factor of 2. However, it is still appreciably higher than that of the incoherent radiator and much of the radiation can still be collected by a short length cylindical optic.

The randomizing effects of the electron beam emittance can cause further deteriorization of the peaks of the annulus. In Fig. 3.8 we show cases where larger emittances are used. These are given in the figure caption. As we can see from the figure, the annulus can disappear as the beam quality deteriorates. High quality (low emittance beams) can be obtained with conventional linac and microtrons (see for example table 7.1, for the microtron).

3.4.3. Elastic scattering

The number of foils one can use to generate TR is limited by the deterioration of the electron-beam quality as the electrons suffer elastic coulomb scattering from the atoms of the foil material. Changing the direction of the electron beam by elastic scattering will also change the direction of the x rays. Thus when the electrons pass through the foils and suffer collisions their directions are altered and the angle of emission (or half angle) of the x-ray photons is also altered. Spread in the electron beam results in a spread in the generated x rays, decreasing the radiation brightness. Since we are interested in keeping the brightness as high as possible, we wish to minimize the total amount of scattering. To do this the total amount of scattering is limited by reducing the total number of foils or foil stacks that are used. Since the angular width of the RTR annulus is given by Eq. (16), we wish to keep the total scattering to be less than:

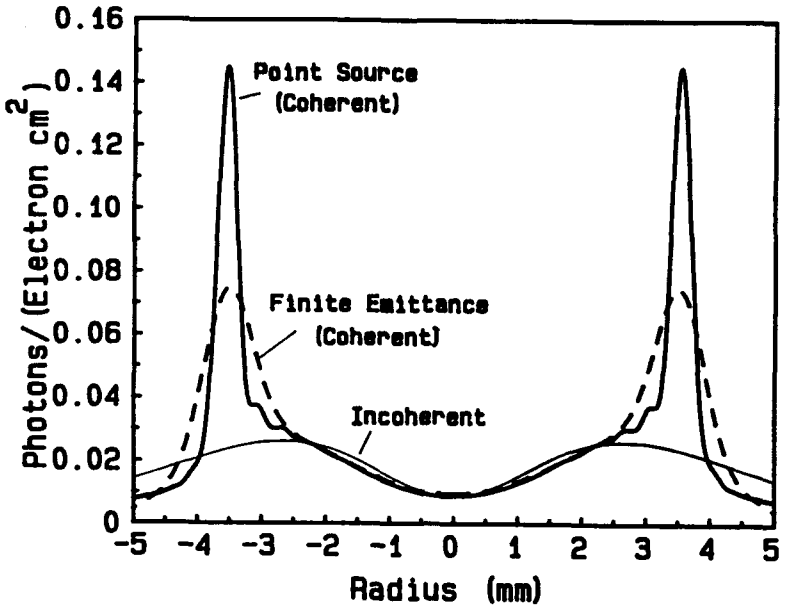

Fig. 3.7. The calculated x-ray spatial distribution from a coherent transition radiator with electron beams of finite emittance compared to an incoherent radiator. The three curves are: (a) coherent radiator with $\epsilon = 0$, (b) coherent radiator with finite emittance $\epsilon = 0.15\pi$ (d = 0.5 mm, $\Delta\theta = 0.6$ mrad), and (c) incoherent radiator. The electron-beam energy is 100 MeV. The foil stack is composed of 19 foils of 2.7 μm titanium spaced 10.8 μm apart. The incoherent radiator has identical foils with large spacing: $\ell_1 = 500$ μm

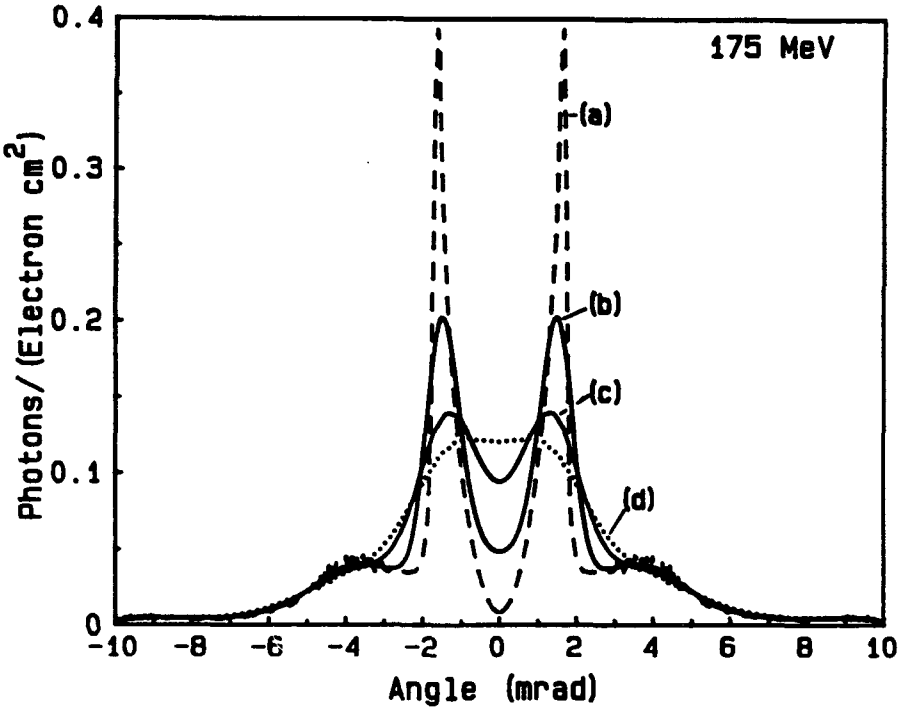

Fig. 3.8. The calculated x-ray spatial distribution from a coherent transition radiator with electron beams of finite emittance. The four curves are: (a) $\epsilon = 0$, (b) $\epsilon = 0.15$ mm-mrad, (c) $\epsilon = 0.6$ mm-mrad, (d) $\epsilon = 1$ mm-mrad. The electron-beam energy is 175 MeV. The foil stack is composed of 35 foils of 6.4-μm mylar spaced 30 μm apart (used in the experiments discussed in section 6)

$$\theta_S < 0.4\sqrt{\frac{\lambda}{M\ell}} \tag{22}$$

then the angular width of emission of the photon beam will be roughly

$$\theta = \sqrt{\theta_S^2 + \frac{0.16\lambda}{M\ell}} \tag{23}$$

Thus if the $\theta_S = 0.4(\lambda/M\ell)^{1/2}$, the total amount of angular spread on the transition radiation cone will be only increased by a factor of $\sqrt{2}$, and the total area that the X rays strike will be increased by a factor of 2. The power per unit area will be decreased by a factor of 2.

The total amount of foil material that the electron beam must go through is given by the product $M\ell_2$, where M is the number of foils in a stack and N is the number of stacks. A reasonable approximation to the amount of scattering in this length is given by the projected angular spread due to multiple scattering:[55]

$$\theta_S \simeq \left[\frac{7.8}{E}\right]\left[\frac{M\ell_2}{X_0}\right]^{1/2}\left[1 + 0.16\log_{10}\left[\frac{M\ell_2}{X_0}\right]\right] \tag{24}$$

where E is the electron-beam energy in MeV, X_0 is the radiation length of the foil material, M is the number of foils and ℓ_2 is the foil thickness. Substituting the equation for scattering into the condition $\theta_S < 0.4(\lambda/M\ell)^2$ and neglecting the last term of Eq. (24) (an extremely rough approximation) and solving for the number of foils, we get:

$$M < \left[\frac{E}{15}\right]\left[\frac{\lambda X_0}{\ell_2(\ell_2 + \ell_1)}\right]^{1/2} \tag{25}$$

As an example, we pick a beryllium foil stack designed to be resonant for 1 keV photons. The maximum number of foils permitted to be used as given by Eq. (25) is 22. For 2 keV photons, the maximum number of foils is 18.

For higher density foils such as titanium as shown in Fig. 3.7, the scattering angle is approximately 1 mrad, as given by Eq. (24), and as shown in Fig. 3.7. In that figure, the angular width (FWHM) of the annulus for a point-source electron beam is on the order of 0.5 mrad. Thus the scattering would broaden the annular width. However, the amount of scattering is overestimated, since the formula given by (24) requires $M\ell_2/X_0 > 10^{-3}$. We are in a regime where there are less than 20 scattering events in the stack (plural scattering) and, thus, the spread in angles due to scattering is smaller than that indicated by Eq. (24).[55]

3.5. BANDWIDTH REDUCTION

A major thrust of this program was to find methods for the bandwidth reduction of transition radiators without the use of monochromators. The use of a conventional Bragg-crystal x-ray monochromator with input and output slits would result in the loss of much of the x-ray flux.

Two methods were explored by us, these are:

1. The use of phase interference inherent between foil interfaces was found to give some reduction in bandwidth. The radiation was found to be dispersive allowing some reduction in bandwidth when the resonance radiator is combined with a cylindrical optic.

2. Quasimonochromicity can be achieve by designing the transition radiator at the photoabsorption edge of the foil material. Effectively integrating a K-edge filter with the radiator resulting in bandwidths of 30 to 60 %. This effect first utilized by us using incoherent radiators. Under this AFOSR-SBIR program, we have investigated the use K-edge designs to limit the bandwidth of coherent radiators. For the first time, we have observed bandwidth narrowing using Zn and Mo foil incoherent transition radiators in Nov. 1991. This technique is discussed in the next section.

3.5.1. Photon absorption-edge bandwidth narrowing

3.5.1.a. Design of K-edge radiators

Previously, we noted that the bandwidths of carbon and aluminum incoherent transition radiators were narrowed by their K-shell photo-absorption edges.[19] In more recent work we show that using high density foils such as gold, stainless steel, and copper permits the electron beam to be of the moderate energy (100-500 MeV) while still producing warm to hard x-rays.[20] Combining these two ideas, one can design transition radiators to emit quasi-monochromatically throughout the x-ray spectrum by selection of an appropriate K-, L- or M-edge material.[21]

The bandwidth of the K-edge radiator can be reduced by a factor of 2 or more when compared to that of a transition radiator which is not designed at the K- or L-edge. Since the x-ray absorption is reduced on the low frequency side of the K- or L-edge, the number of foils that one can use can be large, permitting intense x-ray production. Since each element of the periodic chart has different K-, L-, and M-edge frequencies, one can design foil stacks across the x-ray frequency keV band. Using lithium foils we can obtain 55-eV photons, while using gold foils we can obtain 80-keV photons. Radiator designs are given in table 3.1 whose frequency bands span the soft and warm x-ray region. The calculated spectral power density using a 100-μA electron beam is plotted in Fig. 3.9 as a function of x-ray photon energy for the four radiators of Table 3.1. Bremsstrahlung radiation is included in the calculation. The spectra of the Al, Ti and Zn are optimized to have peak emission at their respective K-shell photoabsorption edges, while the Be radiator is not. The Be stack is designed to resonate at 2 keV. We plan to construct these radiators in Phase II.

3.5.2.b. Measured spectral photon density from Ti, Zn and Mo radiators

Under an DOE-SBIR we measured the spectrum of the emitted x rays from a titanium, zinc and molybdenum incoherent transition radiators using pulse height analysis (PHA). The measurements of the zinc and molybdenum radiators was made during the period of this AFOSR contract and have been

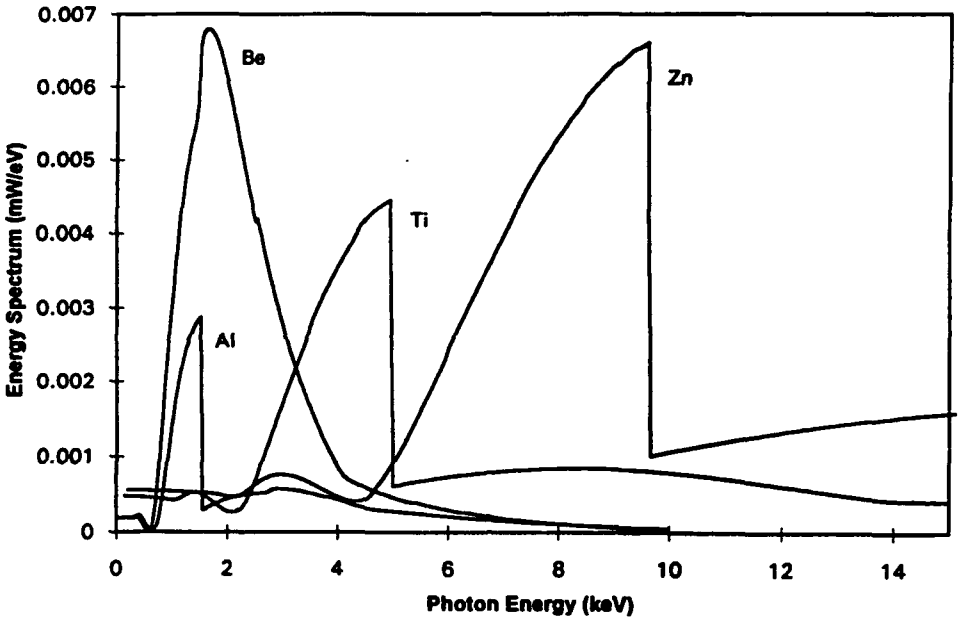

Fig. 3.9. The spectral power density of four stacks composed of foils of beryllium, aluminum, titanium and zinc each optimized at their respective K-shell photoabsorption edges. The beryllium is optimized at 2 keV. The parameters for the four stacks are given in table 3.1. The average beam current is 100 μA.

TABLE 3.1
Design Parameters for RTR stacks

	Al	Be	Ti	Zn
PLASMA FREQ. eV.	32.9	26.1	41.5	52.2
FREQUENCY eV.	1560.0	1500.0	4960.0	9600.0
ELECT. ENERGY MeV	70.0	70.0	150.0	270.0
FOIL THICKNESS μm	1.44	2.02	2.68	3.52
FOIL SPACING r=1 μ	7.5	7.8	10.8	18.0
ABSORPT. COEF 1/μm	0.105	0.031	0.039	0.026
NO. FOILS	13	32	19	22
MAX SPACING ERROR	0.9	0.6	1.1	1.7

not published. The NPS linac was used for the titanium radiator to supply an electron beam of 90.2 MeV, while the SAL linac was used for the molybdenum and zinc radiators at 270 MeV.

The transition radiators used in the experimental work are given in Table 3.2. For comparison and to extract the data from the background radiation (e.g. ionizations from upstream slits, radiation in the end station), single foils of each material whose thickness was equivalent to the total thickness of the foil stack (e.g. 60 μm of Mo) were used to produce same amount of bremsstrahlung and background radiation as that of the transition radiator.

The PHA of the spectral photon density was performed using a Si(Li) detector for the titanium

TABLE 3.2
FOIL STACKS USED IN THE EXPERIMENT

FOIL MATERIAL	Ti	Zn	Mo
K-absorption edge, keV	5.0	9.7	20.0
Electron Energy, MeV	90.4	270.0	270.0
Foil Thickness, μm	2.0	3.0	4.0
Number Foils, M	10	15	15

stack, while a NaI detector was used for the zinc and molybdenum stacks.

The calculated and measured spectra for the Ti, Zn and Mo foil stacks are shown in Fig. 3.10 The spectra do not show the sharp drop in the x-ray flux at the K-edge because of the frequency resolution of the detectors. The general shape of the measured spectrum matches that of the calculated ones.

The data shows clearly that the K-shell photoabsorption edge does indeed narrow the bandwidth of the radiator. This is the first time that such high-density foils have been used to generate transition radiation.

3.6. DESIGN OF RESONANCE TRANSITION RADIATORS

3.6.1. Types of resonance radiators

Previously, we constructed resonant structures as shown in Fig. 3.11. This RTR stack was made from an assembly of eight concentric steel rings. The rings were cut from steel tubing and ground flat and parallel to the same thickness. Type "C" mylar (Trademark of E. I. Dupont de Nemours Inc.) was epoxy bonded to the face of each ring. The smallest mylar-covered ring was bolted to a flat-ground steel plate. The next larger ring was attached similarly, with the addition of shims between two mating surfaces to space the adjacent mylar foils by a distance equal to the shim thickness minus the foil thickness. The resonance stack contained 8 foils with a nominal foil thickness of 3.5 μm and a nominal foil separation of either 8.5 or 5 μm. For RTR to be bright source of x-rays, the number of foils used must be large. Unfortunately, achieving a larger numbers of foils (M >8) is difficult to achieve using this approach.

In order to increase the number of foils we have studied two radiator designs. These are categorized as follows:

1.) Foil stacks made of low or low density materials such as Be or mylar with vacuum spacing.

2.) Foil stacks made of laminated materials of alternating high and low density materials such as Cu and polypropylene.

As will be discussed in the next section and in section 6, we have successfully constructed and tested a

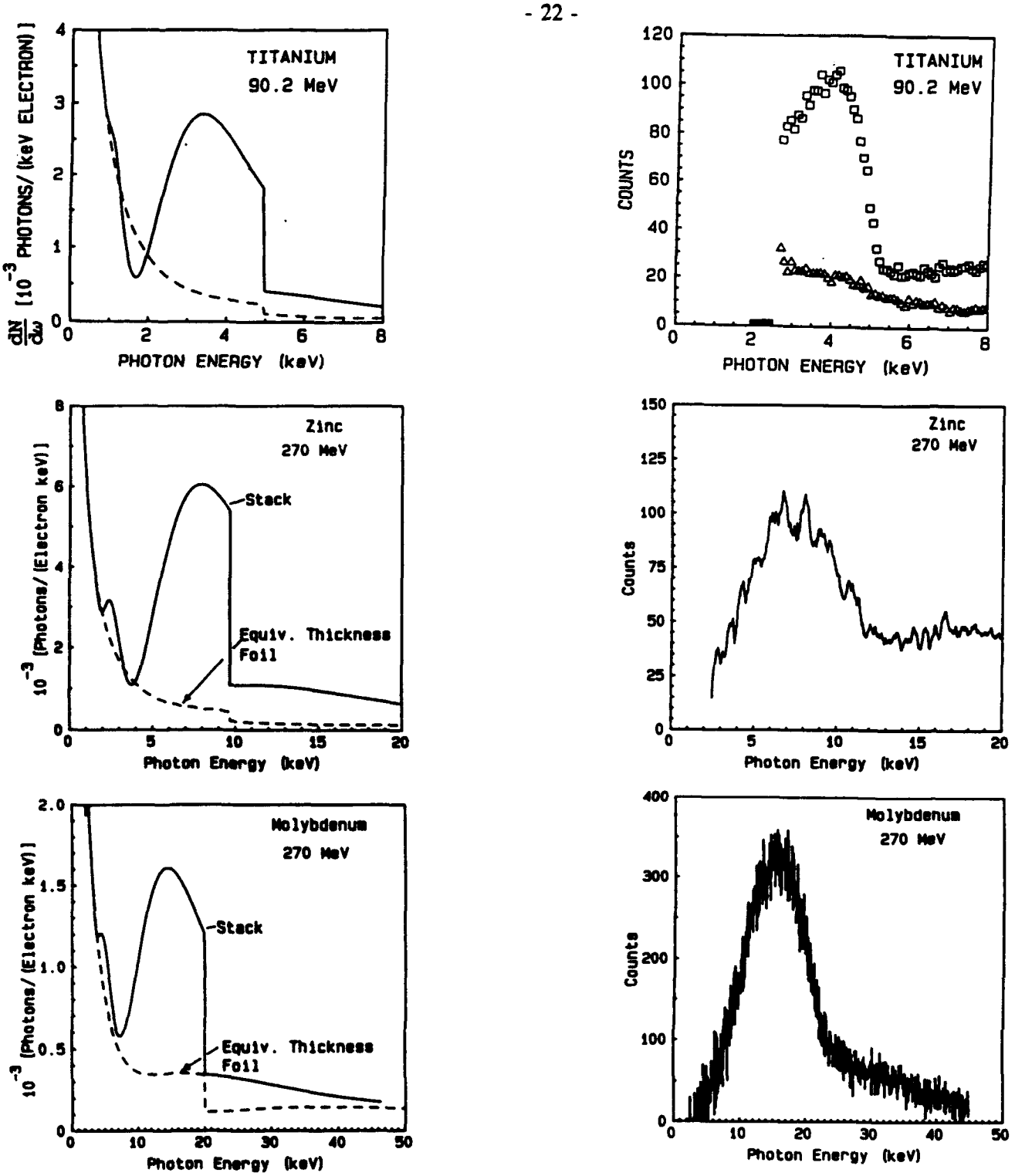

Fig. 3.10. The (a) calculated and (b) measured spectra from titanium, zinc, and molybdenum radiators. The measured radiation from the equivalent-thickness foil has been subtracted from measured radiation from the foil stacks (shown for the Ti case).

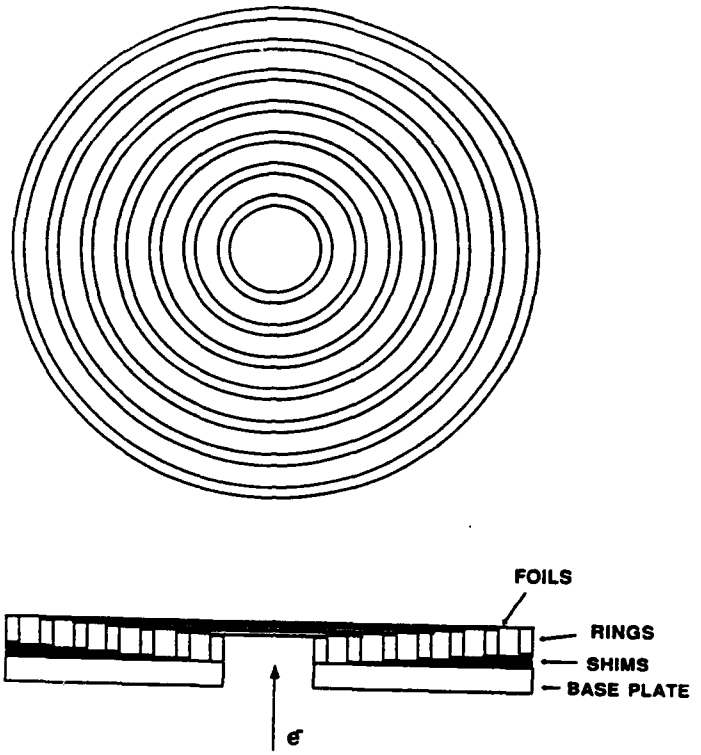

Fig. 3.11. The concentric ring RTR mylar-foil stack composed of an 8-ring stack with three sets of steel shims placed 120 degrees apart. The shims determined the interfoil spacing, ℓ_1. This method is probably limited to 8 foils or less. This radiator was used in work discussed in refs. 10,11,13

35 foil radiator utilizing mylar with vacuum spacing.

3.6.2. Solid/vacuum laminated RTR radiator

A simple radiator design would require foils interspaced by thin spacers for support. In actual construction, this has proven difficult in the past. However, as we discovered in our phase I analysis of nonuniform stacks, discussed in section (3.3), the error in spacing can be fairly large without to much alteration in the angular dispersion. Therefore, we constructed resonance radiators composed of laterating layers of thin mylar and punctured stainless steel. A diagram of one of the two radiators is shown in Fig. 3.12. The radiator was composed of 6.4-μm mylar which was glued over thin 25-μm stainless steel foils 25 x 25 mm in area which had been punctured by 1 -cm diameter holes. The stainless steel foil was sufficiently rigid and the adhesive was viscous enough that the mylar could be stretched tightly over the 1-cm hole without the mylar foil shrinking and the stainless steel bending. Individual mylar/stainless-steel foils were then stacked on top of one another and the entire structure squeezed between two plates that had 1-cm diameter holes coaxial with those of the stainless-steel foils. The thickness of each individual mylar/stainless-steel foil was measured using a digital micrometer whose stated accuracy by the manufacturer was ± 0.5 μm.

3.6.3. Solid/solid laminated RTR radiator

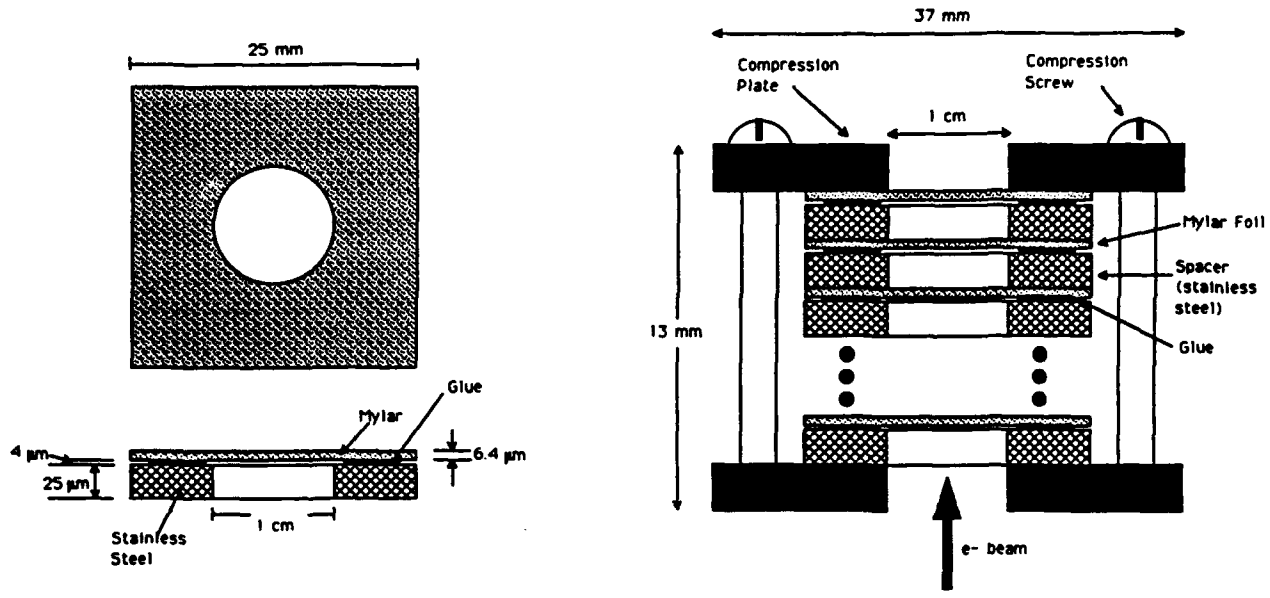

Fig. 3.12. A laminated radiator consisting of mylar and stainless steel shims. (A) is a single foil with spacer. (B) is the complete stack. This radiator, constructed under this contract, was used in the November and February experiments at SAL.

TABLE 3.3

TRANSITION RADIATORS CONSTRUCTED UNDER PHASE I

TYPE	$\ell_2(\mu m)$	$\ell_1(\mu m)$	M
Coherent	5.0	50	30
Coherent	6.4	35	35
Incoherent	6.4	≈135	35

Another method for obtaining a larger number of accurately spaced foils would be a laminated medium composes of alternating foils of moderate and low density foils. Such a structure would be easier to construct, and be more compact and rugged. Most importantly it would give more accurate foil spacings. A possible drawback would be that the solid/solid single-interface photon production would be smaller than that of a medium/vacuum interface.

Two method exist for construction laminated medium. One method utilizes a technique used for the construction of synthetic Bragg scatters for soft x-ray monochromators. These structures called layer synthetic media (LSM) have been researched by Barbee and others. The LSM is constructed by vapor deposition of alternating layers of materials. Alternating layers of, for example, tungsten and carbon have been constructed. Spacings of 15 Å up to 1 μm have been achieved. Such radiators with

spacings on the order of a micron would be ideal for compact RTR radiators for threshold detectors of hadrons. Both the principal investigator and others have investigated these structures for transition radiation.[57,58] The principal investigator has collaborated with Barbee in the construction and testing of an LSM structure composed of Mg and C. This device was tested at NPS in the late 1970's, and a small amount of transition radiation was observed (unpublished). The number of foils was small, and the signal relatively small.

Another method for obtaining a laminated medium would be to obtain single foils of the proper thickness, stacking alternating foils one on top of another such as done in the construction of capacitors. Vapor depositing a metal on a plastic could also be used. The coated plastic would then be cut into sections and stacked. Aluminized mylar is an example of a coated plastic. A threshold radiator composed of alternating layers of aluminum and mylar can be constructed since this technology has been developed for capacitors. Thin aluminized mylar can be purchased in sheets of threshold (0.5 m x 10 m).

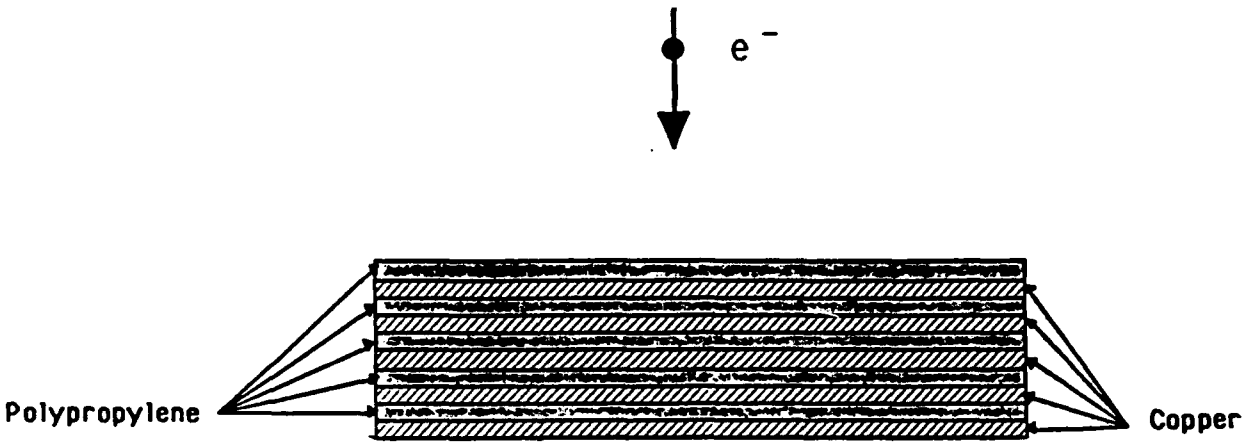

Fig. 3.13. A laminated radiator consisting of polypropylene and copper foils. The radiator uses solid/solid laminar construction.

In order to produce the maximum flux obtainable one would like to make the difference in plasma frequencies as large as possible to obtain maximum emission. A moderate density foil such as copper and a low density plastic such as polypropylene as a spacer material appears to be an excellent radiator of RTR. A design for such a radiator is given in Fig. 3.13. The foil thicknesses are approximately 2.5 μm for the copper and 7.8 μm for the polypropylene. The calculated spatial and spectral distributions are given in Figs. 3.14 and 3.15, respectively.

Ed Graper of LeBow Co. has manufactured laminated structures by simply gluing layers of W and C together using light silicon based glue.[59] This can be done with copper and polypropylene. Each layer is pressed together to achieve flatness for a 24 hour curing period.

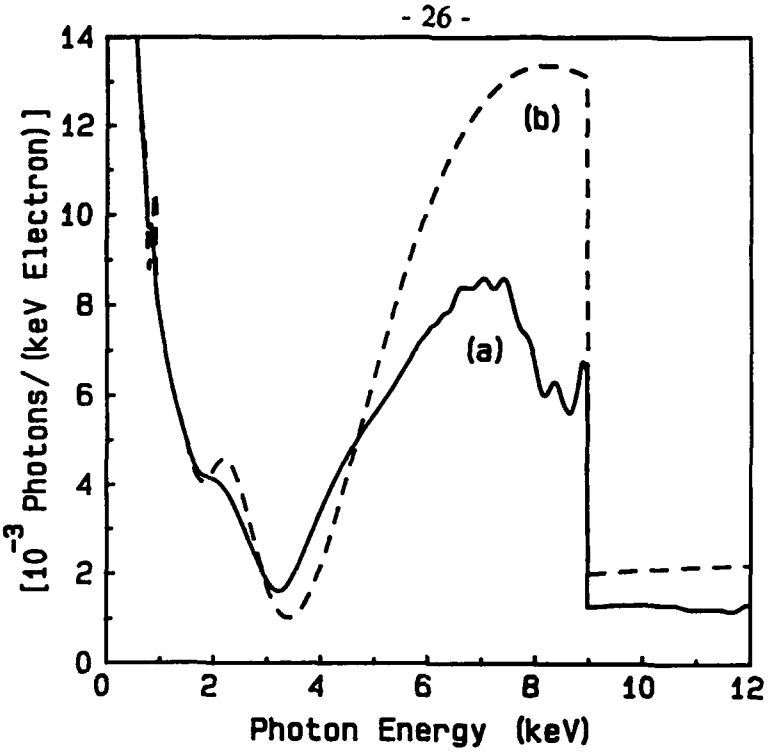

Fig. 3.14. Calculated spectral photon density for (a) 21 foil pair of ℓ_2 = 2.5 μm copper and ℓ_1 = 7.8 μm polypropylene and (b) 21 foils of ℓ_2 = 2.5 μm copper and ℓ_1 = 500 μm vacuum spacing. The electron-beam energy is 447 MeV. The total photon density over the bandwidth from 4 to 9 keV has been reduced by 30%.

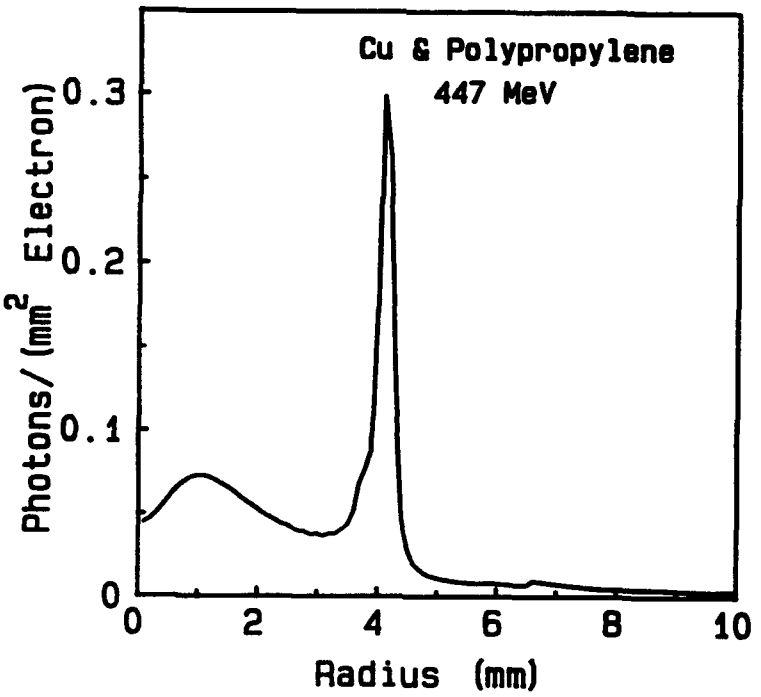

Fig. 3.15. Calculated spatial photon density for 21 foil pairs of ℓ_2 = 2.5 μm copper and ℓ_1 = 7.8 μm polypropylene. Distance from the source to the radiator is 1 m. electron-beam energy is 447 MeV.

4. USING RESONANCE TRANSITION RADIATION WITH CYLINDRICAL OPTICS

4.1. CYLINDRICAL OPTICS FOR FOCUSING

4.1.1. Grazing incidence optics

The intensity (watts/cm^2) of transition radiation can be dramatically increased by focusing the annular radiation pattern with grazing incidence optics. Reflection at grazing incidence is possible because at x-ray wavelengths materials have an index of refraction less than unity. Indeed, the index of refraction for a medium at x-ray wavelengths can be written as:[29]

$$n = 1 - \delta - i\beta \tag{26}$$

where δ and β are positive, and where β is a measure of x-ray absorption.

For small or negligable β, total reflection from vacuum-to-medium (or air-to-medium) occurs if the incidence angle θ is less than the critical angle θ_c, where:[29]

$$\theta_c = \sqrt{2\delta} \simeq \frac{\omega_p}{\omega} \tag{27}$$

and where ω_p is the plasma frequency of the medium and ω is the radiation frequency. Here the incidence (grazing) angle is defined as the angle between the reflecting surface and the incoming x-ray beam. As an example, for quartz ω_p = 33.2 eV, so that 2 keV photons will be highly reflected when striking a quartz surface at angles $\theta < \theta_c$ = 16.6 mrad.

Transition radiation is emitted in an annulus which diverges conically at a small apex angle θ, which goes roughly as the ratio of the electron's rest energy E_0 to the electron's total energy E (e.g. for 50 MeV electrons, the apex cone angle is approximately 10 milliradians and the spot size is approzimately 2 cm in diameter at a distance 1 m from the source). By virtue of this small-diverging, annular radiation pattern, transition radiation is well suited for focusing by grazing incidence optics with azimuthal symmetry (rotational symmetry about the radiation axis), as is qualitatively depicted in Fig. 4.1. The optic can be a simple cylinder or tube, or more complicated surfaces such as ellipsoids, hyperboloids, or some combination of the above. In general, the optic should be designed to intercept as much of the transition radiation (at angles $\theta < \theta_c$) as possible. In what follows, we describe the design and testing of a simple cylindrical optic.

4.1.2. Design issues for cylindrical optics

An important function of the optic is to intercept as large a fraction of the emitted TR as possible. The solid angle that a cylindrical optic with radius r, length L and distance z from the source (see Fig 4.2), intercepts is given by the expression[42]

$$W = \frac{1}{\sqrt{1 + \left[\frac{2r}{2z + L}\right]}} - \frac{1}{\sqrt{1 - \left[\frac{2r}{2z + L}\right]}} \tag{28}$$

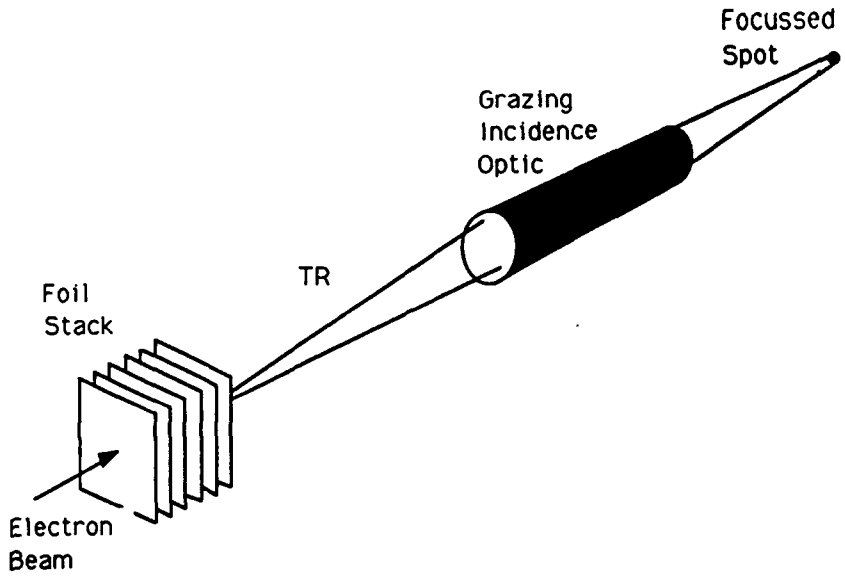

Fig. 4.1. A qualitative depiction of the use of grazing incidence optics to focus transition radiation. Because the radiation is emitted in an annular pattern, simple cylinders and ellipsoids are ideally suited for collecting the radiation.

Differentiation yields

$$\frac{\partial W}{\partial z} < 0 \text{ and } \frac{\partial W}{\partial r} > 0 \tag{29}$$

so that in general the optic collects more flux with larger values of r and smaller values of z. Note, however, that Eq. 28 describes the solid angle an optic will intercept, but in fact the transition radiation is not evenly distributed in space. For non-resonant TR, the emission is roughly confined between angles $1/2\gamma$ and $3/2\gamma$ to the beam axis, where γ is the Lorentz factor for the electrons, so that the above guidelines hold only within this range of angles (indeed, in practice one will choose the beam energy γ and the optic position so that the peak emission angle, roughly $1/\gamma$ for incoherent radiators, will hit the center of the optic). In addition, the optic will only be effective for grazing angles $\theta < \theta_c$; so this is an additional limit on r and z (for increasing radius r and/or decreasing distance z, the grazing angle θ increases). Finally, there may be practical constraints limiting r and z such as the vacuum pipe diameter and the distance between the source and the detector in the experimental setup.

A second function of the optic is to direct (focus) the collected radiation to a small region of space. Simple geometry dictates that the optic be centered between the source and detector, and furthermore indicates that for a source of radius r_s, detector of radius r_d, source-to-detector distance of D, and cylindrical optic radius r, the useful length of the cylinder L is given by (refer to Fig. 4.2)

$$L = D \frac{2r_m r_d + 2r_m r_s}{2r_m^2 - (r_d - r_s)^2} \tag{30}$$

That is, radiation striking the cylinder beyond this length L will not be directed to the detector with

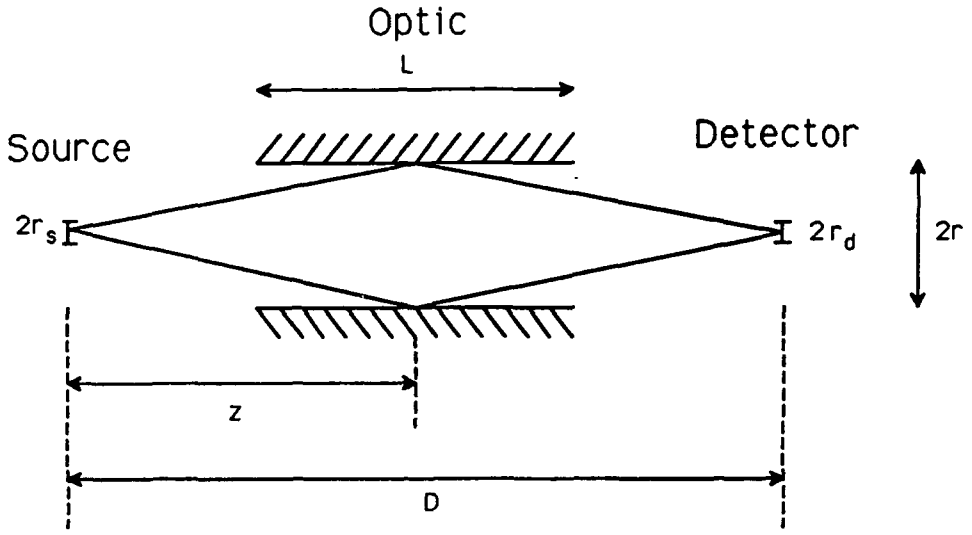

Fig. 4.2 Side view of a focusing system using a cylindrical optic, showing the relevant dimensions (the size of the optic is greatly exaggerated here).

radius r_d. In general, r_s, $r_d \ll r$, so that

$$L_{max} \simeq D\left\{\frac{r_d + r_s}{2r_m}\right\} \tag{31}$$

As an example, for an experiment performed at SAL under a DOE phase II project (described in next section), we designed our optic for a source-to-detector distance D = 3 m, estimated the electron-beam size r_s = 1 mm, and took r_d = 1 mm. This meant that for a cylinder length L ≃30 cm, we needed r greater than 1 cm. We actually used a 1' (≃30 cm) long quartz tube with an inner diameter of 1" (≃1.27 cm). The larger radius allows for slightly greater flux collection while still keeping $\theta < \theta_c$. Indeed, for these dimensions the grazing angle along the optic will vary between 7.6 and 9.4 mrad, while the critical angle for quartz is 16.6 mrad for 2 keV photons. Finally, for a non-resonant foil stack, the peak emission angle is roughly $1/\gamma$; this implies approximately 60 MeV for the beam energy in order to hit the center of the optic.

4.2. EXPERIMENTAL RESULTS OF FOCUSSED TRANSITION RADIATION

We tested the quartz cylinder optic (a described above) at the Saskatchewan Accelerator Laboratory (SAL) using a non-resonant stack consisting of 12 foils of 1 μm thick aluminum and another consisting of 10 foils of 2 μm thick titanium; for both stacks, 75 MeV electrons were used to generate the TR. To learn more about the focussing properties of the cylindrical optics, we also tested a second optic, having the same dimensions of the quartz tube, but with a nickel surface. Besides having a different optic material, the nickel optic also had a different value for the surface roughness. The surface roughness is typically described by the rms variation in the surface height σ (above or

below the mean surface position); for the quartz optic $\sigma \simeq 6$ nm while for the nickel optic $\sigma \simeq 10$ nm.

In the experiment, the optics were centered on-axis 1.5 m from the source, and a scanning diode array at 3 m from the source was used to view the resultant radiation pattern. For each case, a focussed peak was found, and 1-D traces through the peaks are shown in Figs. 4.3. corresponding to the four different combinations of radiators and optics. The different traces for each case correspond to different measurements. and their variations are attributed to errors in focusing as well as uncertainty in the current measurements. The highest flux occurred for the quartz optic with the Al radiator, and was approximately 185 W/A-cm^2 (averaged over the 1 mm diameter spot). For the SAL beamline, an average current of about 0.13 mA (36 mA peak) can be obtained at 75 MeV, resulting in a flux of 2.4 mW/cm^2 (6.7 W/cm^2 peak).

It is interesting to compare this result with calculations based on simple geometry. For a cylindrical optic, the radiation that is collected into a 1 mm diameter spot at the detector plane is just that which would have otherwise gone into an annulus of width 1 mm and mean radius equal to the optic diameter (see Fig. 4.4). Thus we expect that the increase in flux due to the optic is equal to the ratio of the annulus to spot area. This can easily be shown to be given by the ratio 16r/d, where r is the optic radius and d is the diameter of the spot. For our experiment this ratio is $\simeq$200. The measured value of 185 W/A-cm^2 using the quartz optic and the Al radiator is an increase of $\simeq$175 times over the flux in the absence of the optic, based on computer simulations. Thus it is evident that in this case the measured increase in flux is close to the theoretical ideal, and so absorption in the optic as well as surface roughness effects did not degrade the focussing properties of the optic significantly.

In general the effects of surface roughness and material absorption on the focussing will depend on the x-ray energy as well as on the particular choice of optic material. A fuller discussion of these effects, including an analysis of all the data taken at SAL is given in the following section.

4.3. SURFACE ROUGHNESS EFFECTS ON REFLECTIVITY

A common treatment of surface roughness effects on x-ray reflectivity is to use an approach analogous to the treatment of displaced lattice effects on x-ray scattering. In this analysis, first taken by Debye,[43] the attenuation of the reflected intensity is given by

$$\frac{I_d}{I_\mu} = \exp\left\{-\left[\frac{4\pi\sigma\sin\theta_i}{\lambda}\right]^2\right\} \tag{32}$$

where σ is the rms variation in the surface height (above or below the mean surface position), λ is the x-ray wavelength and I_d and I_μ are the attenuated and ideal intensities. The validity of this model is that the first Fresnel zone is much larger than the mean period of the roughness $\ll\!>$(parallel to the surface), that is, for[29]

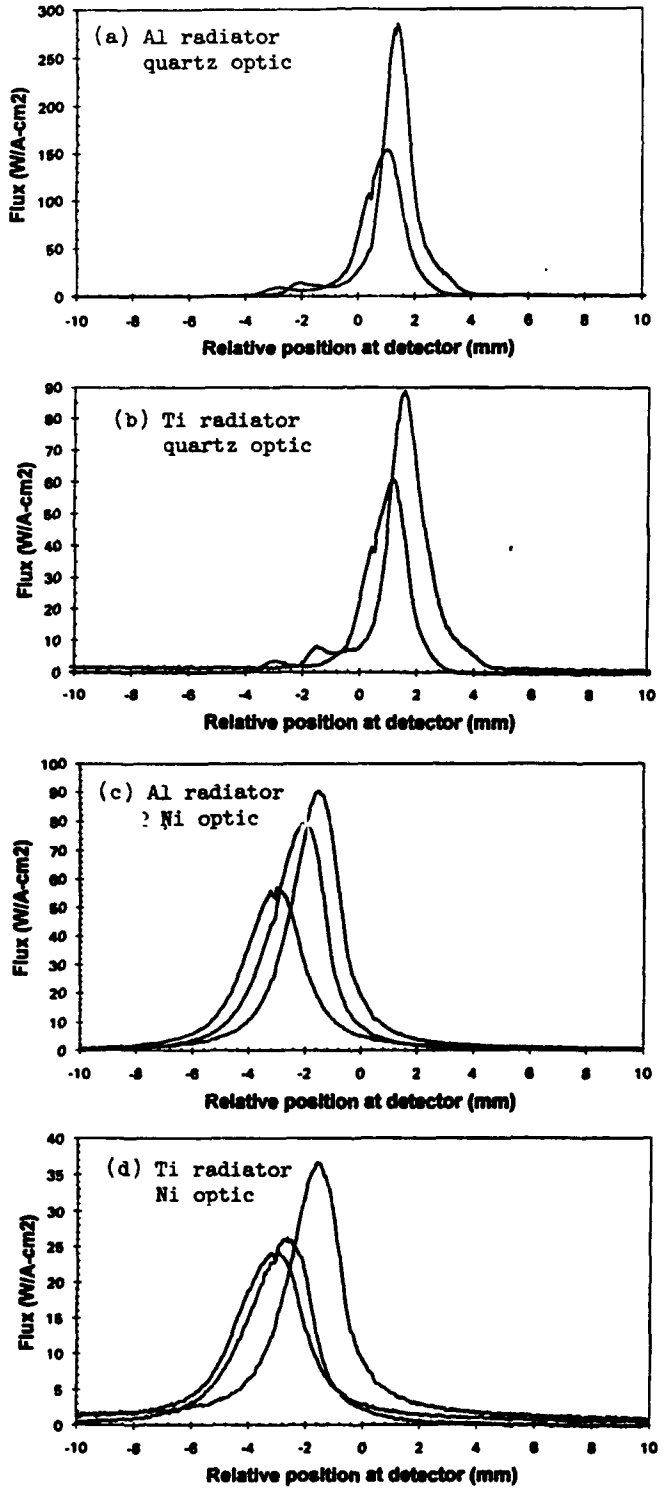

Fig. 4.3. The measured results of the cross sections through the focused peaks for different combinations of sources and optics. (a) Al radiator with quartz cylindrical optic, (b) Ti radiator with quartz optic, (c) Al radiator with nickel optic, (d) Ti radiator with nickel optic.

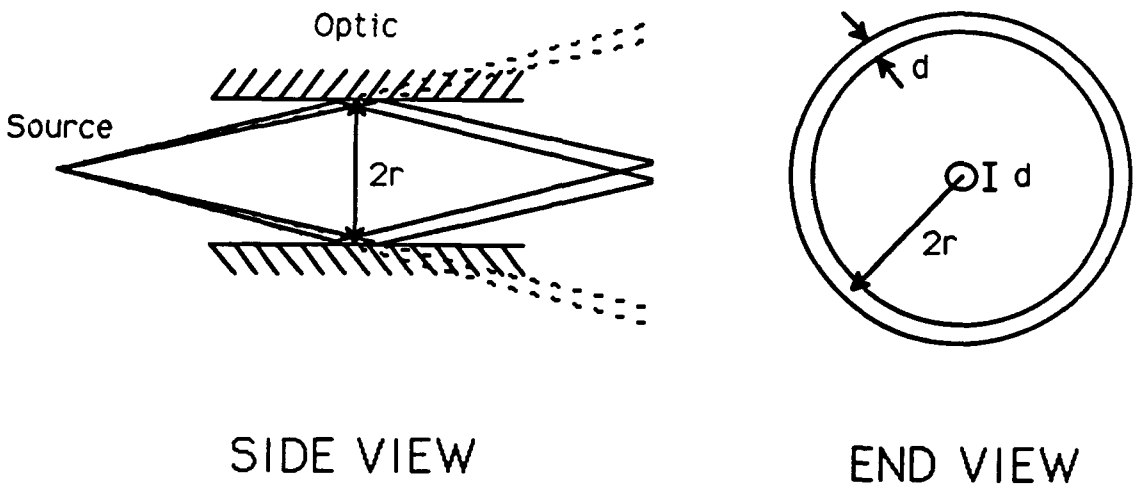

Fig. 4.4. A side view of a cylindrical optic focussing system. Extreme rays that get collected to a spot of diameter d are drawn. These rays would, in the absence of the optic, form the outline of an annulus of width d and radius 2r, where r is the optic radius.

$$\langle s \rangle = \frac{\sqrt{\pi\sigma\lambda}}{\sin\theta_i} \tag{33}$$

This condition is certainly satisfied in transition radiation where θ_i is on the order of mrads. The total reflectivity is then reduced by the factor I_d/I_μ given in Eq. 32, commonly known as the Debye-Waller factor.

A partial understanding of the form of this factor can be had by reference to Fig. 4.5, which depicts x-rays reflecting off of two surfaces, displaced by a distance σ. The difference in phase between the two rays can easily be shown to be equal to $4\pi\sigma\sin\theta_i/\lambda$. Since high intensity reflection depends on constructive interference of the reflected x-rays, it is clear that the reflectivity will be reduced for larger values of $4\pi\sigma\sin\theta_i/\lambda$, and this is precisely what is indicated by the Debye-Waller factor. Note that in particular the reduction is greater for shorter wavelengths, that is, for harder x-rays, since a given difference in path length is a larger phase difference.

The Debye-Waller factor cannot be applied indiscriminately, however. Several investigators have shown that the surface roughness of metal and glass surfaces do not significantly reduce the reflectivity, particularly for hard x-rays.[44-49] Indeed, Bilderback and Hubbard have shown that an imperfect surface of unpolished (rolled) sheet copper surprisingly reflected as much as 50% of incident x-rays out to 9.0 keV at a grazing angle of 3.5 mrad,[28] whereas the Debye-Waller factor would have predicted virtually no reflection.

In what follows we present a simple model for determining when and when not to apply the Debye-Waller factor for calculating grazing incidence reflectivities, that is, the model determines when surface roughness effects are or are not important. It turns out that both the x-ray photon

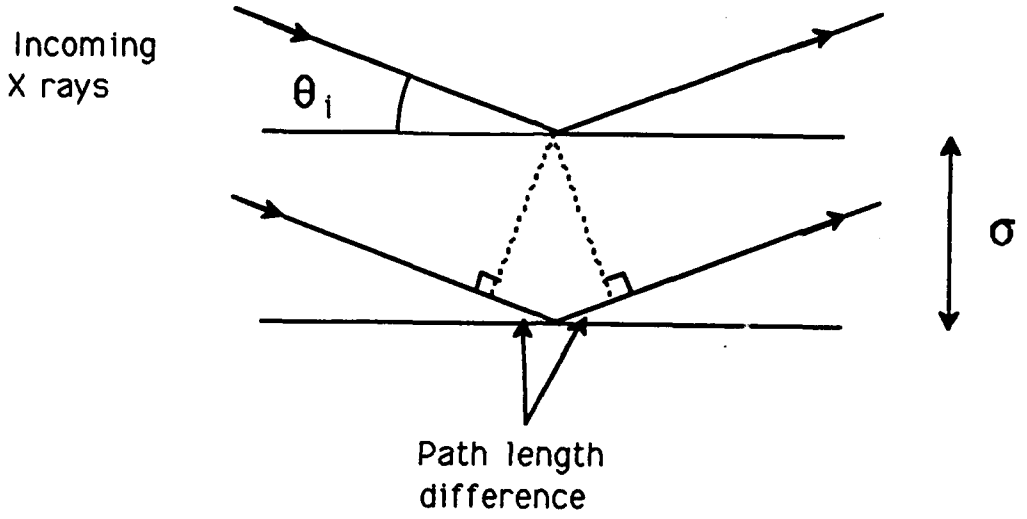

Fig. 4.5. A diagram showing the path length difference between x-rays reflecting off from two different surface heights.

energy as well as the optic material are important in this determination. This model adequately explains the experimental data taken at SAL, and this is also discussed below.

The model can be best understood with reference to Fig. 4.6. When x-rays impinge on a surface, they interact with the molecules in that surface, and the resultant "re-radiation" of the interacting molecules is what causes reflection. Only molecules within some depth D of the surface interact, however, and this depth can be small (Fig. 4.6a) or large (Fig. 4.6b) compared to the roughness σ. For $D \ll \sigma$, the interacting layer follows the surface roughness, and thus roughness effects are important in determining the reflectivity. For $D \gg \sigma$, the roughness is only a small perturbation on the overall (smooth) surface, and roughness effects are less important. In summary, using this simple model, we expect that roughness effects become more important with increasing value of the parameter σ/D.

The depth D depends on the x-ray absorption of the material; the absorption determines how far into the surface the x-rays penetrate, and thus the depth of the interacting layer. As a rough measure, we take the depth as the position where the x-ray has diminished by a factor 1/e. Then we have

$$D = \frac{\lambda}{4\pi\beta}\sin\theta_i \tag{34}$$

where β is the imaginary part of the index of refraction. In general, β will depend both on the material as well as on the photon energy. For virtually all materials β is reduced faster than λ with increasing energy (see for example, Fig. 4.7 which plots β versus photon energy for the two materials used in our SAL experiments, nickel and quartz), so that the interacting layer D increases for harder x rays. This implies that in general roughness effects diminish for harder x rays. Counteracting this, however, is the fact that the Debye-Waller factor (Eq. 32) results in a greater reduction for harder x rays.

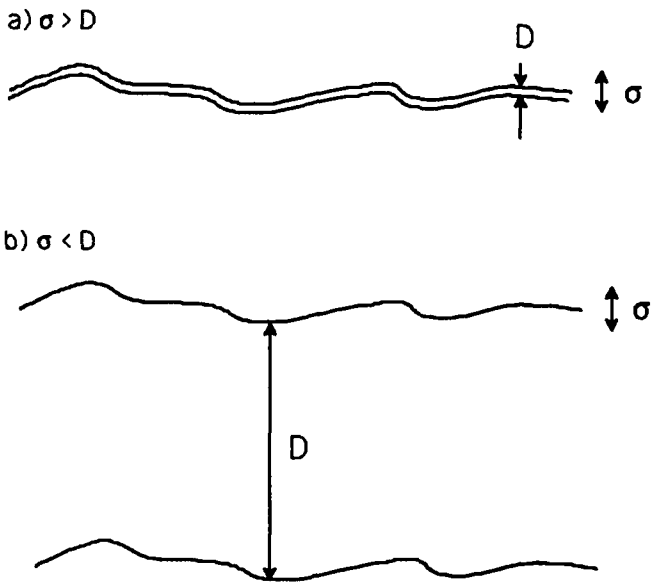

Fig. 4.6. The depth D of the "interacting" layer of a surface with roughness s. a) D $\ll\sigma$; the interacting layer conforms to the surface roughness. b) D $\gg\sigma$; the roughness is only a small perturbation to the smooth interacting layer.

This suggests that appropriate choice of the optic material and roughness can serve as a frequency filter on the reflected radiation; both very long and very short wavelengths are reflected, the very long wavelengths because the Debye-Waller factor is close to unity, and the very short wavelengths because the Debye-Waller factor no longer applies. Indeed, this effect can be used to improve the bandwidth characteristics of the x rays beyond what is described in section 4.7.

4.4. SURFACE ROUGHNESS EFFECTS IN THE EXPERIMENTAL DATA

As described earlier in Section 4.1, measurements were made at SAL using quartz and nickel focussing cylinders with Al and Ti radiation sources. It is useful to see how our simple model of surface roughness effects compares with the real effects seen in the experimental data.

In fact our simple model explains the experimental data quite well. In Table 4.1 the measured fluxes for the different combinations of TR sources and focussing optics are shown, as well as results from computer simulations performed at Adelphi Technology. Also shown is the ratio σ/D for each of the four cases. D was calculated assuming a mean photon energy of 3.5 keV and 1.2 keV for the Ti and Al radiators, respectively, and σ was measured experimentally ($\sigma = 6$ nm for the quartz optic and $\sigma \simeq 10$ nm for the nickel optic). The simulation results assume a beam emittance of 0.25 mm-mrad, as well as take into account x-ray absorption of the optic. For each case, a simulation was performed with and without roughness effects (i.e. with and without the Debye-Waller factor). We find that for all cases, the measured flux falls between the two simulation results, but that for small values

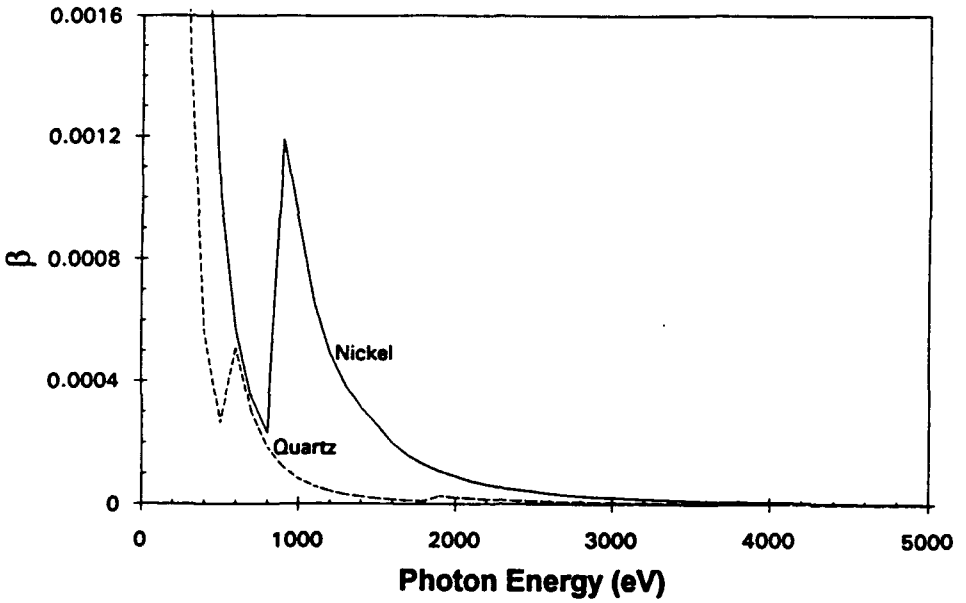

Fig. 4.7. The imaginary component of the refractive index β, as a function of energy, for quartz and nickel.

of σ/D the simulation without roughness effects best approximates the real data, while for larger values of σ/D the simulation including roughness effects is better. This is precisely what is predicted by our simple model. In particular, we see that for the quartz optic the roughness is not important, whereas significant improvement in flux can be had by reducing the roughness of the nickel optic. In phase II we will investigate different methods of improving the surface roughness of the optic.

TABLE 4.1
COMPARISON BETWEEN MEASURED AND CALCULATED FLUXES FROM FOCUSSED TRANSITION RADIATION

Foil	Optic	σ/D	Average Measured Flux (W/A-cm^2)	Calculated Flux (W/A-cm^2)	
				w/ roughness	w/o roughness
Ti	Quartz	0.06	52.5	15.8	61.9
Al	Quartz	0.29	149	75.0	151.4
Ti	Nickel	0.47	23.3	10.0	81.4
Al	Nickel	6.94	60.7	40.3	181.5

4.5. ADVANTAGES OF RTR FOR FOCUSING

We mentioned earlier that the small-divergence annular pattern of transition radiation is well suited for capture by grazing incidence optics. Indeed, neither synchrotron radiators, conventional x-

ray tubes, nor laser-plasma sources can have as much of their radiation patterns to be collected as transition radiation. However, even for transition radiation the amount of radiation that a cylinder can intercept and bring to a focus is limited, because of limitations on the length of the optic. The optic length is constrained both because of geometrical concerns as described by Eq. 31 but as well as from practical concerns in terms of construction ability. Since the x-rays emitted from incoherent radiators have a finite spread in angles, the limitation on optics length means that the amount of radiation intercepted may only be a small fraction of the total flux available in the annulus.

A RTR source, however, can be designed to emit in the r = m = 1 resonance mode, making the angular spread of the radiation extremely small. If this emission is then passed through a well designed cylindrical optic, the total amount of collected and focussed x-rays can be greatly increased. Almost the entire thin annular ring can now be intercepted by the cylindrical optic.

Indeed, we have performed computer simulations of focusing using a quartz cylinder optic on the radiation from two foil stacks consisting of 26 2.5 mm-thick Be foils, and using a 150 MeV electron beam. The difference between the stacks is that one has random foil spacing (non-resonant) while the other has a fixed interfoil spacing of 21.8 mm (resonant). To best approximate a real situation, we have included a finite emittance on the electron beam (0.3 mm-mrad; the SAL beam emittance can be controlled by collimating slits, 0.3 mm-mrad is a typical value), and also included absorption of the radiation by the quartz tube as well as the reduction of the reflection coefficient due to surface roughness on the optic. We took as the surface roughness 5nm, which is what is measured for the quartz optic we used experimentally (see section 4.4 for a discussion of surface roughness effects). The position and dimensions of the optic were chosen to cover the FWHM of the RTR radiation pattern. This leads to the optic having a radius of 1.3 cm, lying between 236.9 and 325.8 cm from the source, and with the detector at 526.3 cm from the source (note that these values can all be scaled without changing the results). Figs. 4.8a and 4.8b show the radiation pattern at the detector, for different electron-beam parameters. In Fig. 4.8a the beam has a radius of 0.5 mm and an angular divergence of 0.6 mrad, while in Fig. 4.8b the radius is 1.0 mm and the angular divergence is 0.3 mrad. In both figures the resonant or coherent stack produces a higher flux concentration than the non-resonant or incoherent stack, by factors of 4 to 6. Results are summarized in Table 4.2.

Also included in Table 4.2 are values for peak intensity and FWHM for an electron beam with virtually no emittance. Clearly, the emittance is the dominant factor in determining the quality of the focussed radiation; the peak intensity drops by a factor of 16 when the real SAL beam emittance is used (as opposed to an ideal beam), and the FWHM of the spot grows roughly proportionally with the beam radius. For the same beam emittance, however, the RTR always focuses to a greater peak intensity spot than the non-resonant TR.

Finally, it should be noted that for non-cylindrical optics such as an ellipsoid, longer lengths can

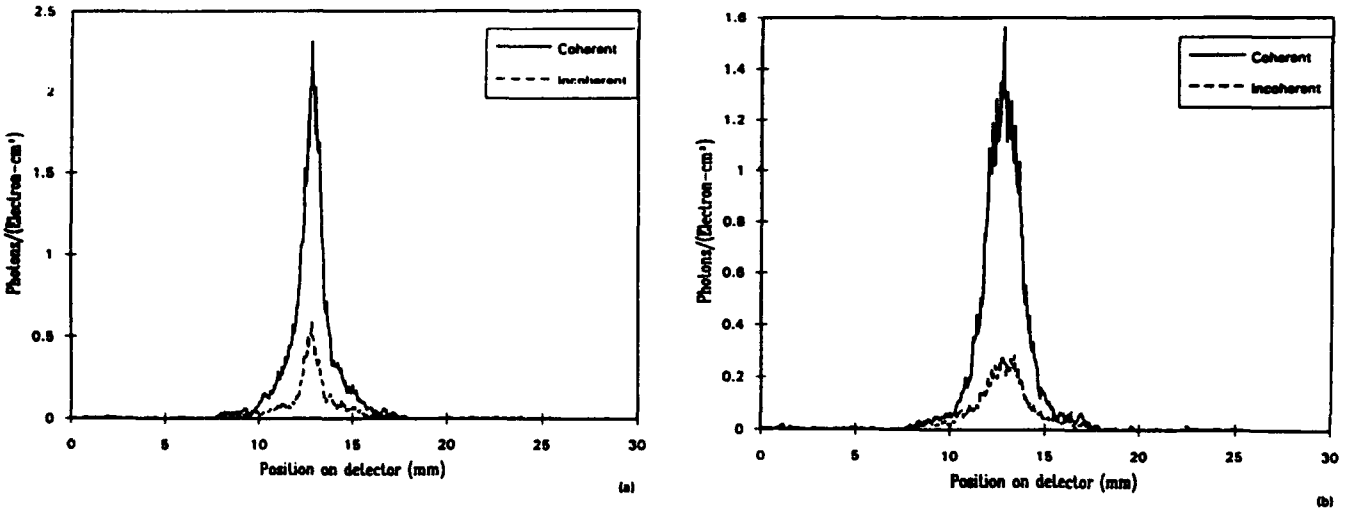

Fig. 4.8. Calculated spatial distribution of a focussed beam spot from resonant and non-resonant radiators. a) Beam radius = 0.5 mm, beam angular divergence = 0.5 mrad b) Beam radius = 1.0 mm, beam angular divergence = 0.3 mrad. The radiators were composed of 26 foils of 2.5 μm Be, spacing for the RTR stack was 21.8 μm, and $\simeq$500 μm for the incoherent stack. E = 150 MeV.

TABLE 4.2
COMPARISON BETWEEN FOCUSSED SPOTS FROM COHERENT AND INCOHERENT TRANSITION RADIATION.

Beam parameters	Peak intensity (photons/electron-cm^2)			FWHM (mm)		
	Resonant	Non-Resonant	Ratio	Resonant	Non-Resonant	Ratio
0.01 mm 0.0 mrad	36.9	4.35	8.5	0.05	0.05	1.0
0.5 mm 0.6 mrad	2.305	0.586	3.9	0.95	0.9	1.05
1.0 mm 0.3 mrad	1.56	0.281	5.5	1.85	1.95	0.95

be used and still direct radiation to a small region of space (this is due to the well-known property of the ellipse in which a ray emitted at one focus will be reflected and travel through the other focus). Thus there is no geometrical limit to the useful length of the optic analogous to Eq. 4.31 for the cylinder. However, fabrication of ellipsoidal optics is difficult, and in practice its length (i.e. aspect ratio) is limited by construction constraints. In addition, insertion and alignment of the optic can be problematic for longer lengths. In summary, the thinner annular ring of coherent TR permits the construction of reasonable size optics, and this is beneficial independent of the optic shape.

4.6 ELLIPSOIDAL OPTICS

Thus far we have only considered cylindrical optics. An ellipsoidal optic is expected to offer certain advantages due to its well known property that all rays emanating from one focus will be reflected to the other focus; that is, if we have a point source, and that source is located at one focus of the ellipse, all collected radiation will be brought to a single point at the other focus. Such an optic will be especially useful in applications such as Laue diffraction studies of biological materials in which the spot size of the radiation is required to be small. In addition, we expect that since the radiation is collected into a smaller spot, the ellipsoid will in theory produce a higher peak flux. However, an elliptical walled optic with circular cross section is more difficult and more expensive to fabricate than a straight walled tube, which are commercially available (for quartz and glass) in various diameters and lengths. In addition, the ellipsoid has more stringent tolerances in terms of optic alignment than the cylinder, which does not actually bring diverging rays together, but rather redirects them toward a central region.

The design of the ellipsoidal optic is governed by the following three equations:

$$b = a\sqrt{1 - e^2} \tag{35a}$$

$$D = 2ae \tag{35b}$$

$$e = -\tan(\theta - \phi)\sin\phi + \cos\phi \tag{35c}$$

where a and b are the semi major and semi minor axes of the ellipsoid, respectively, D is the source to detector distance (the separation of the foci), θ is the grazing angle, and ϕ is the radiation angle. All these dimensions and angles are depicted in Fig. 4.9.

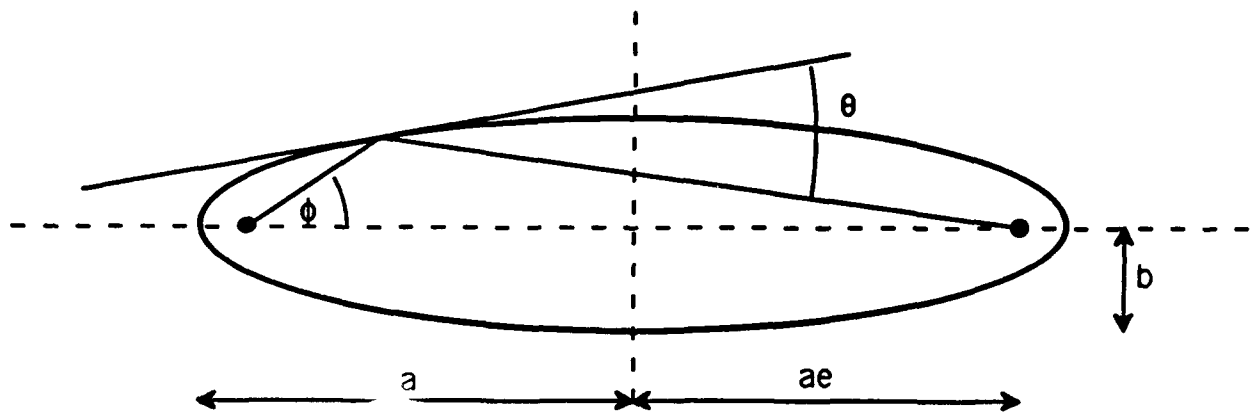

Fig. 4.9. An ellipsoidal optic for focusing RTR showing its major dimensions. Here the vertical dimension is greatly exaggerated as compared to what would be used in practice.

It is known that the majority of the transition radiation is found for radiation angles $1/2\gamma < \phi < 3/2\gamma$ (for coherent radiators, this range will be narrowed), and so the eccentricity e must be chosen so that over this range, or over some fraction of this range, the grazing angle θ determined by Eq. 5.4c) is less than θ_c. It turns out that Eq. 5.4c) sets a lower bound on the value of e. Once a choice for the eccentricity e is chosen, values for a and b follow from Eqs. 5.4a-b), for a given source to detector distance D. The shape of the ellipsoid is then given by the polar equation

$$r = \frac{a(1 - e^2)}{1 - e\cos\phi} \tag{36}$$

where r is the distance from the source to the surface of the ellipsoid.

Of course, in practice only a section of the ellipsoid's total surface can be constructed (again, this is why RTR is advantageous as a source; its radiation pattern is narrow, so a large fraction of the total flux can be captured by a short optic), and so there remains the choice of which section will be used as an optic. In general it is better to take a section of the ellipsoid closer to the source, since a given optic length will capture a greater solid angle there. Of course, this choice must be made in conjunction with the choice of radiator and electron beam energy, as well as with the physical constraints of the experimental set-up.

In pevious work, we constructed an ellipsoidal optic similar to the nickel cylinder described in Section 4.1 and 4.2. We tested the ellipsoidal optic, and were able to find a focussed spot. However, the intensity of the spot was significantly less than what we expected, and actually less than what was obtained using cylindrical optics. We attribute this to the large roughness of the ellipsoid. The roughness of the ellipsoid was estimated by measuring test flats fabricated using the same process used for fabricating the ellipsoid. The test flats had roughness $\sigma \simeq 15$ nm, and since in general curved surfaces will have greater roughness than flats, we expect this value to be a lower bound.

5. COMPARISON BETWEEN TRANSITION AND SYNCHROTRON EMISSION

5.1. SIMULATION OF SYNCHROTRON RADIATION

Synchrotron radiation is the electromagnetic radiation emitted by a charged particle moving with relativistic velocity through an external magnetic (or electric) field. Our simulation takes on the case in which the charge is an electron and it is moving on a circular orbit. The calculated field is at a large distance from the electron orbit in the forward direction of the electron motion. We use the formulas derived by Hofmann.[35] Integrating these formula, we can obtain both spectral and spatical distributions. The output is in the unit of (keV or photons)/(Electron-(eV or radian)) vs (keV or mrad).

5.2. COMPARISON OF RTR WITH SLAC SYNCHROTRON RADIATION

5.2.1. Source differences are important

Comparison of synchrotron with other sources must be done with care, taking into account each sources limitations both in their physical design and electron beam parameters. For example, synchrotron radiators require electron beam eneryies of a few GeV in order to obtain soft x-rays while RTR requires energies on the order of 50 to 300 MeV. Knowledge of each source's spatial and spectral characteristics is essental and the sources specific application is important. For example, if a small x-ray-spot size is required for a specific application, as in Laue diffraction, either the souce must exhibit a high degree of collimation, or x-ray optics must be employed for focusing. Synchrotron sources achieve collimation by operating at extremely high electron-beam energies and by spatial filtering (slits). Our TR source achieves similar results using the resonance effect with cylindrical optics.

An important limitation is the electron beam current. Transition radiators are limited to an average current of a few hundred μA, whereas the synchrotron sources routinely achieve currents between 40 to 250 mA, a factor of 10^3 more. In our analysis given here, we compare first fluxes on a per electron basis and then brightness with practical but unequal currents and energies.

5.2.2. Production efficiency

When comparing x-ray sources, one simple unit of comparison is the production efficiency (defined as the number of photons generated per unit bandwidth per incident electron). In Fig. 5.1, we compare an RTR radiator with that of the Stanford Synchrotron Radiation Laboratory's (SSRL) 12.7 m radius synchrotron source operating at 2 GeV. The transition radiators are composed of 81 foils of 3.2 μm beryllium and 22 foils of 3.38 μm Zn. The RTR source has been optimized at 2 keV and utilizes a 150-MeV electron beam. We compare RTR sources with the simple bending magnet (the radius of the electron orbit is 12.7 m.). The total number of photons is obtained by integrating over area of the annulus ($\theta \simeq \pm 20$ mrad) for the TR source and over the synchrotron lobe ($\theta = \pm 20$ mrad, $\phi \simeq \pm$ 0.5 mrad, where ϕ is the angle in the horizontal plane). Most of the photon energy is in forward direction with an angular width of about $1/\gamma = 0.17$ mrad. As can be seen from the figure, the production efficiency is a factor of 10^2 to 10^3 higher above that of the synchrotron source. However, since the electron beam current can be 10^3 larger for the synchrotron source, the total number of photons generated per keV is about the same.

5.2.3. Brightness Comparison

For applications such as spectroscopy, Laue diffraction, and microscopy, a high brightness source is required. The unit of "brightness" is conventional and familiar to workers in this field, but it can paint an unduly gloomy picture of TR. This is due primarily to the larger divergence of the x-rays from transition radiators when they are operated at a much lower electron-beam energies than synchrotron emitters. Since the angle of divergence of both sources goes roughly as $1/\gamma$ for both sources

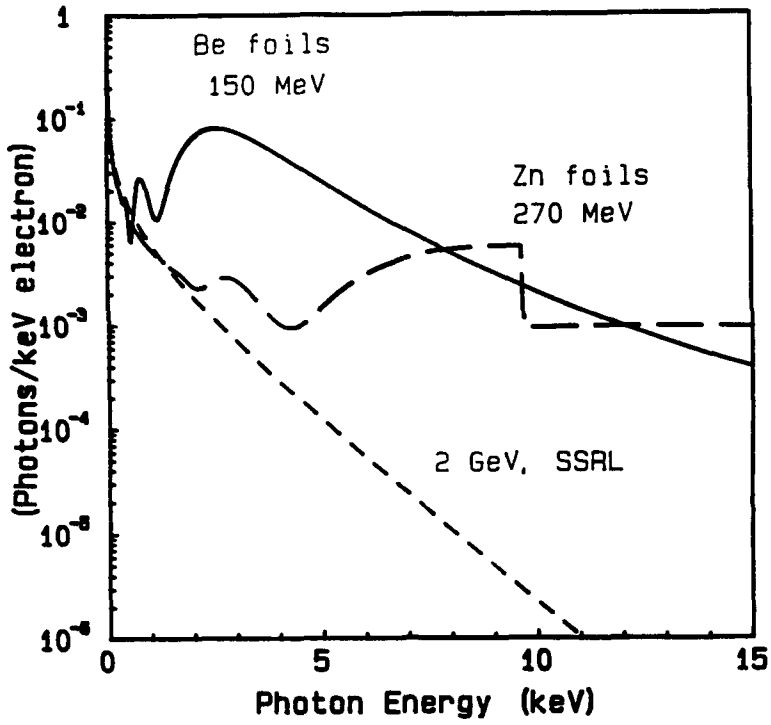

Fig. 5.1. Comparison between production efficiency from a beryllium foil stack and SSRL synchrotron radiator. The Beryllium stack consists of 81 foils of 3.75-μm thick and 21.4 μm apart. The electron energy is 150 MeV. The Zinc stack has 22 foils of 3.38 μm thick and 19.2 μm apart. The electron energy is 270 MeV for Zinc stack. Electron energy is 2 GeV and the sweeping angle is set to 1 mrad. SSRL bending magnet has an electron radius of 12.7 m.

(in one plane for synchrotron sources), the brightness of the lower electron-beam-energy transition source is less than that of the synchrotron's. Since we wish to minimize the cost of a transition source, we must minimize the electron-beam energy. Thus, at first, it appears that brightness of the transition source would be reduced.

During the period of this AF-SBIR contract we have shown that the brightness can be increased by utilizing two methods. Utilizing interfoil phase coherence (resonance) and cylindrical x-ray optics, we can dramatically increase the brightness of the transition source. In addition if we use the pulsed current for the RTR source in the comparison with synchrotron radiators, then the brightness of the RTR source becomes close to that of wigglers.

In Fig. 5.2, we compare the brightness of the two coherent stacks discussed above along with the brightness of SSRL bending magnet and wiggler. The peak brightnesses of the coherent TR are between the wiggler and bending magnet. The electron beam energies and the stack parameters are the same for the RTR stacks as they were in Fig. 5.1. In both cases, the electron current is pulsed at 360 Hz and has a width of 1 μs. Thus the pulse current is 185 mA and the average current is 66 μA. The cross section area of the electron beam is 0.6 mm^2. These are the typical values for the electron beam at SAL.

The typical brightnesses of bending magnets and wigglers at SSRL are given in ref. 54. The electron energy at the synchrotron ring is norminally 3 GeV. The average current at SSRL is about 70 mA. The bending magnets and wigglers at other synchrotron facilities may have different brightnesses. The value for SSRL sources are quite typical.

The figure shows the RTR brightness to be higher than that of the synchrotron source by a factor of 15 at 2.5 keV and just slightly lower than that of the 27-pole wiggler. The major advantage of coherent TR is its lower electron energy and current. Its electron energy is a factor of 20 lower than that of the synchrotron and its average current is more than 1000 times lower than synchrotron.

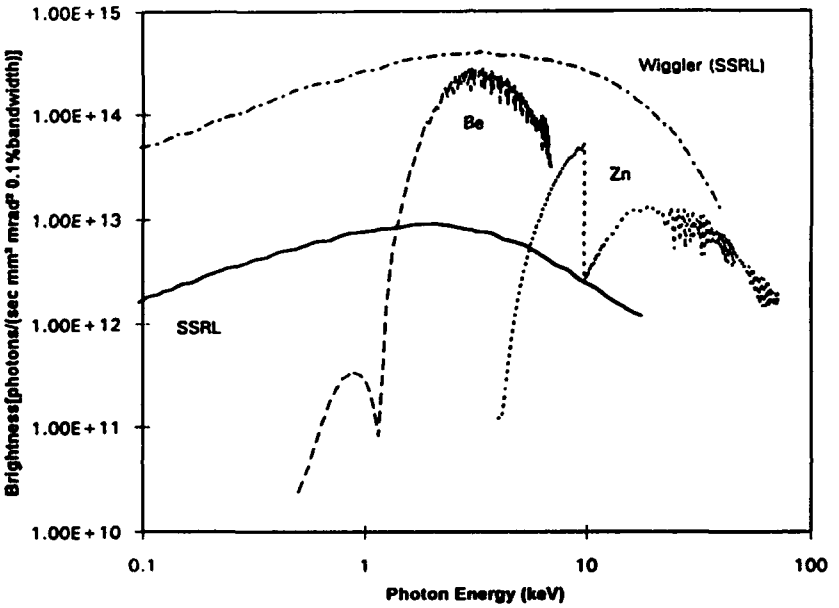

Fig. 5.2. The peak brightness of coherent TR and synchrotron radiation. The parameters of transition radiator stacks are the same as those in Fig. 5.1. The peak pulse current is 185 mA for 1 μs both stacks. The electron energy at SSRL is 2 GeV and the current is 100 mA.

One of the early objectives of the use of synchrotron radiation was to use its inherently pulsed nature combined with its high intensity to permit time-resolved spectroscopy and structural studies. One problem has been that such investigations are feasible only when the electron beam in the storage ring consists of a single, tightly packed bunch of electrons, so that there is time between light pulses to observe the changes in the sample under study. Most synchrotrons operate most easily in a multibunch mode or are so small that the electrons come around the ring too quickly.

Transition radiation offers an alternative method to synchrotron of pulsed, high-peak-power production of x rays. The x-ray time structure is controlled by the electron-beam emitter which can be any of a variety of medium energy accelerators such as a linac, microtron, pelitron, induction accelerator or flash electron source. Each has a unique time structure that may be far more governable or

more optimum for a particular experiment than a synchrotron emitter. For example the Lawrence Livermore National Laboratory (LLNL) linac has a fast-pulse mode in which 12 A electron-beam pulses of between 5 pS to 100 nS can be obtained with millisecond spaces between pulses. X-ray pulses with this time structure would be ideal for studying many transient effects in solids and biological materials.

From these arguements and comparisons, we see that RTR with optics can fill a possible a commercial and scientific niche as a pulsed, quasimonochromatic x-ray source.

6. EXPERIMENTAL CONFORMATION OF RESONANCE

Under this contract two resonance transition radiators with a larger number of foils than previous used were designed, constructed and tested. The construction of these radiators is discussed in section 3, and their parameters given in Table 3.1. For one of the RT radiators, a incoherent radiator with identical foil thickness and number was also constructed and its angular emission pattern compared to that of the resonance emitter. The two radiators could be interchanged in the electron beam quickly permitting a comparison of the spatial distribution for identical electron-beam energy and emittance. The angle of peak emission was found to increase with electron-beam energy, in contrast to the incoherent case, for which the angle of emission varied inversely with electron-beam energy.

Accelerator beam time was obtained during November 1991 and February 1992 from the Saskatchewan Accelerator Laboratory (SAL), at the University of Saskatchewan, Canada. The accelerator can produce a high power (10 kW), moderate electron-beam energy (50 to 300 MeV) electron beam. We utilized beam energies between 157 and 247 MeV.

The experimental apparatus shown in Fig. 6.1 consisted of a foil-stack chamber, dump magnet and x-ray detector. We installed a 6-port vacuum-chamber cube with remotely actuated target holders. Three targets could be placed in the electron-beam path without breaking vacuum: two transition radiation targets and a phosphor screen. Targets could be interchanged in a matter of seconds. We used an existing 90^0-bending magnet for separating the electrons from the x rays, as well as an 8-foot shaft that served as a beam dump.

The angular distribution of 4-keV x rays was observed during every machine pulse with a 2.54-cm linear-diode array (Model No. S2301-512 SPL, windowless version, Hamamatsu Corp.). The array has 512 diodes each, with a photosensitive area of 50 μm by 2.5 mm subtending a solid angle of 6.76×10^{-8} Str at the stack-to-detector spacing of 1.34 m. The array could be translated up to 17 cm in the plane perpendicular to the electron-beam axis. Translating the diode array across the annulus gives the false color plots shown in Fig. 6.2 and 6.3.

In the November run, we use an RTR radiator composed of 30 foils of 5 μm mylar spaced 50 μm apart. The run was terminated early because of radiation damage to the linear diode array. However,

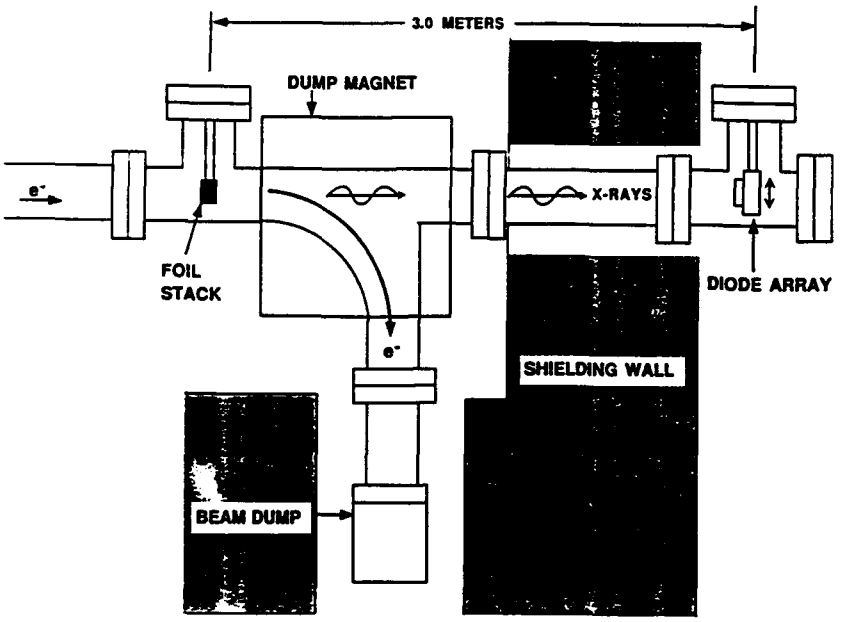

Fig. 6.1. The experimental apparatus for measuring the spatial distribution of the x-rays generated by RTR.

there was time enough to measured the radiator's angular distribution at 282 MeV. This is shown in Fig. 6.2 As can be seen from the figure, the spatial distribution is slightly asymmetric. This asymmetry seems only to appear from resonance emitter and not incoherent radiators.

The shape of the angular distribution and the separation of the radiation peaks from the incoherent radiator case agreed with the predicted theoretical values. As can be seen from the distributions shown in the figure, the angle of peak emission is different for the two radiators.

The radiation distribution was observed at 5 different electron-beam energies between 157 and 247 MeV. From the distributions the angular divergence of the peak emission was measured and plotted as a function of electron beam energy. The results are shown in Fig. 6.4 for the case of the RTR and incoherent stacks. As discussed in section 3.2 and shown in Fig. 3.5, these differ radically: the incoherent case decreases with increasing energy, while that of RTR increases. The RTR case is also dependent upon foil thickness and spacing while the incoherent case is dependent only on electron beam energy. This functional dependence conclusively shows that we are indeed observing RTR.

For one of the RT radiators, a incoherent radiator with identical foil thickness and number was also constructed and its angular emission pattern compared to that of the resonance emitter. The two radiators could be interchanged in the electron beam quickly permitting a comparison of the spatial distribution for identical electron-beam energy and emittance. The angle of peak emission was found to increase with electron-beam energy, in contrast to the incoherent case, for which the angle of emission varied inversely with electron-beam energy. The resonance effect has application in x-ray-source brightness enhancement, x-ray free-electron laser emission, particle detection, and electron-

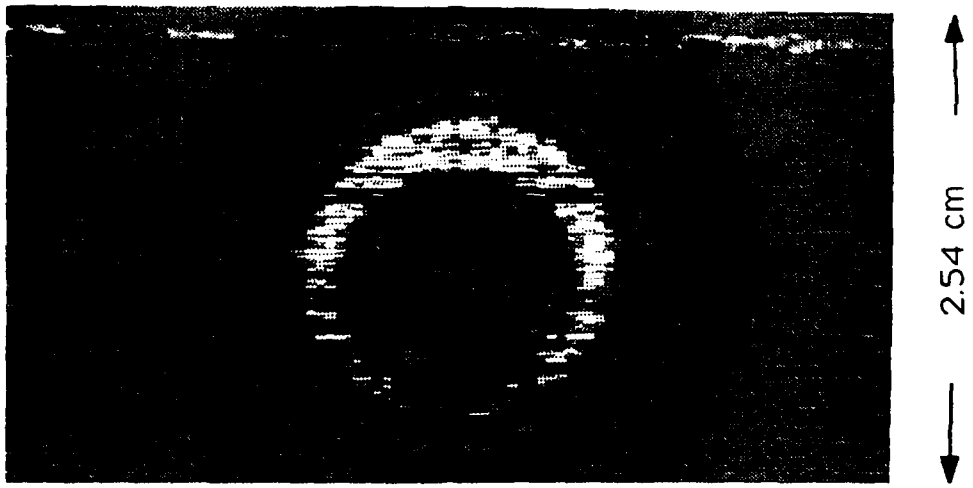

Fig. 6.2. The false color images of the spatial distribution of the RTR stack used during the November run. The electron beam energy was 282 MeV. The color scale follows the visible spectrum with dark red being the most intense and blue-black the least intense.

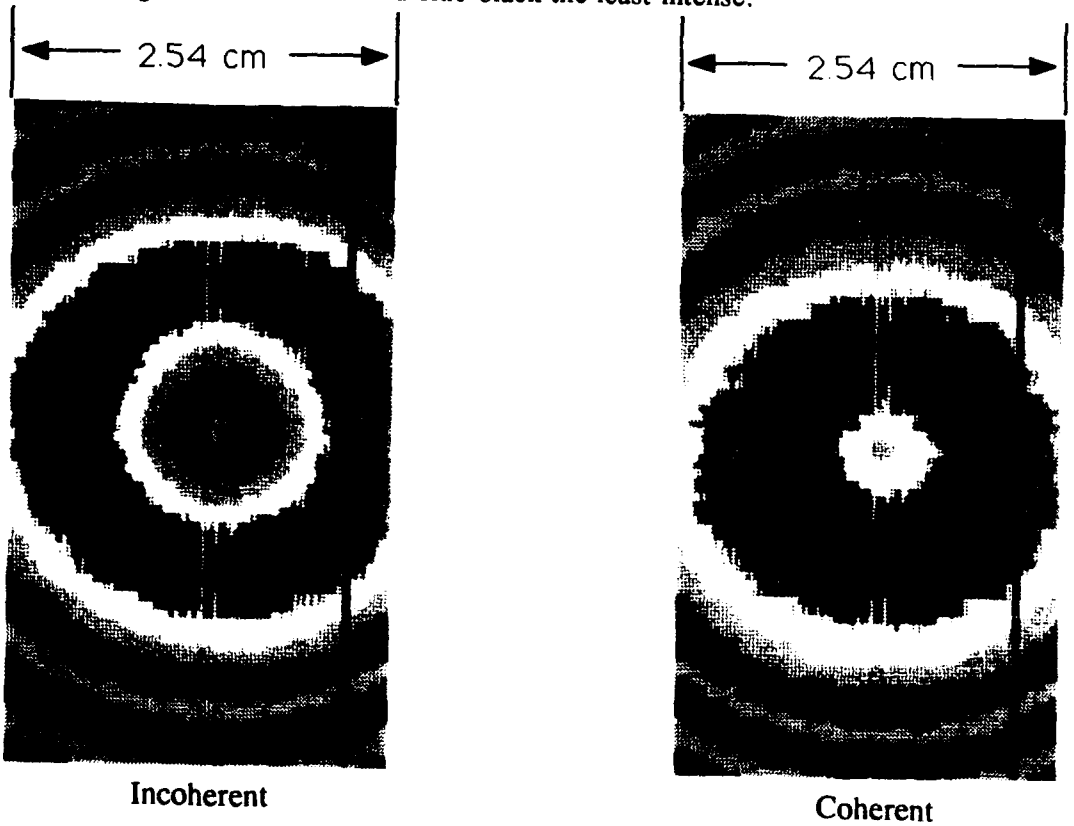

Fig. 6.3. The false color images of the coherent and incoherent radiators at 157 MeV (Feb. 1992 run). The angle of emittance for coherent stack is smaller (1.8 mrad) than that of the incoherent stack (2.7 mrad).

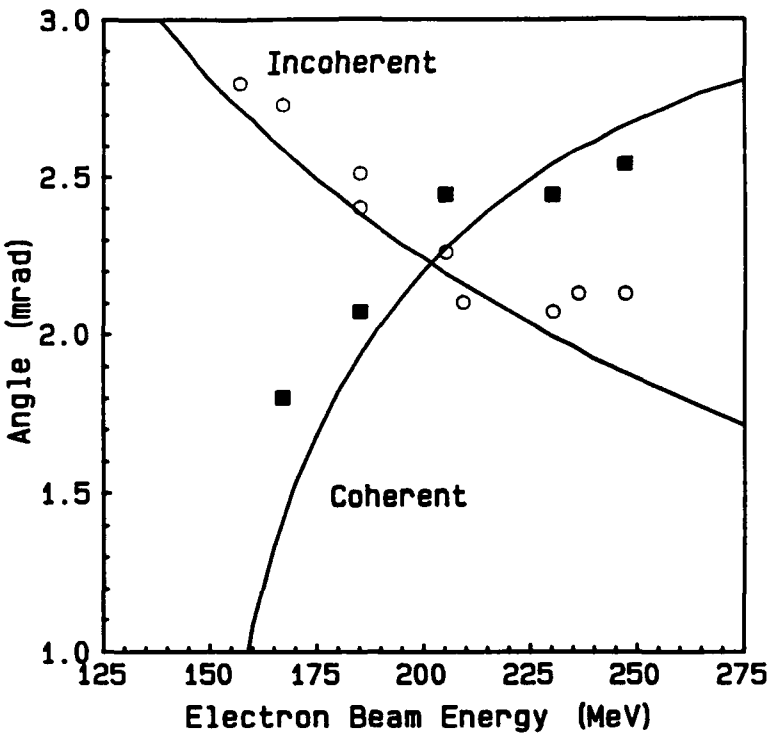

Fig. 6.4. The measured results for the angle of peak emission as a function of electron-beam energy for both incoherent and coherent radiators.

beam diagnostics.

7. COMPACT X-RAY SOURCE USING MICROTRON AND FOCUSING OPTICS

Under this contract, we have considered what a compact x-ray system would consist. Depending upon the energy and beam current requirements of the particular application, we can consider one klystron linacs, pelitrons, and microtrons. The Scanditronix Racetrack Microtron is an attractive possibility. These compact accelerators are capable of emitting relatively high average currents. The Scanditronix system is based on recirculated electron-beam optics. Electrons are injected into a linear accelerator, which accelerates the electrons to 5 MeV. Two dipole magnets, one on each side of the linac, return the beam to the linac to be accelerated again. After each acceleration in the linac the radius of the electron orbit will increase. Finally, the electrons are deflected and extracted. The important characteristics of a racetrack microtron are its small size, high average current, high peak current, small emittance, and low energy spread. These characteristics make the microtron an excellent candidate for a dedicated linac for a focussed transition radiation soft x-ray source.

The size of the model RTM50 accelerator measures 160 x 250 x 80 cm with two modulators in cabinets measuring 200 x 120 x 130 cm each. Three models are available: the RTM50, RTM100, and RTM150. These models have electron-beam energies of 50, 100, and 150 MeV, respectively.

Table 7.1 shows the machine parameters for these accelerators as given by the manufacturer.

TABLE 6.1
Scanditronix Microtron Characteristics

System model	RTM50	RTM100	RTM150
Maximum electron energy (MeV)	50	100	150
Peak macropulse current (mA)	25	15	10
Emittance at maximum energy (> 85% of current)			
vertical (mm x mrad)	0.2π	0.1π	0.07π
horizontal (mm x mrad)	0.2π	0.1π	0.07π
Energy spread at maximum energy (> 85% of current)	$+2X10^{-3}$	$+1X10^{-3}$	$+0.7X10^{-3}$
Macropulse length (μs)	0.05-5	0.05-5	0.05-5
Pulse repetition frequency (Hz)	10-250	10-250	10-250
Maximum Average Beam Current (μA)	31	19	13

A number of transition radiators can also be placed in a single electron beam with bending magnets between each radiator to separate the x rays from the electron beam. The emerging electron beam need not be dumped and could be recycled through the accelerator to its original energy and emittance. Such a scheme could lead to a much lower cost per lithographic station. To minimize cost, one would like to select a one-klystron linac or microtron. The energy of such machines is between 45 and 70 MeV. Microtrons and two klystron linacs can produce 150-MeV electron beams. However, the cost would be almost double that of the 70-MeV linac. As we have seen, using focusing optics with a 70-MeV electron beam is highly desirable.

To decrease the cost per station, additional foil stacks can be added to the electron beam, each with an x-ray beamline and x-ray optics system. Thus the cost per station is reduced by sharing the linac and the electron beam and the users can have incremental increase in production without undue cost. Additional stacks can be added because the electron beam is only slightly perturbed as it passes through the foil stacks. The electrons are elastic-scattered and experience some energy loss as they pass through the foils. However this scattering and loss are minimal for a finite number of foils (e.g. approximately 20 foil stacks of 25 foils of 1 μm beryllium each can be used).

The size of a x-ray system will almost entirely depend upon the size of the electron accelerator. Again, one can consider both linear accelerators and microtrons. An linear accelerator of 50 MeV consists of three major parts of appreciable size: the modulator with klystron measuring 2x3x3 meters, the disc loaded pipe of approximately 2 meters in length, and radiation shielding of approximately 1 meter thick. If a microtron is used then the footprint is smaller.

An example of system for x-ray lithography using a Scanditronix's microtron is shown in Fig. 7.1. The total system is drawn in reduced scale. A synchrotron system requires much larger storage ring and a linac or microtron to supply it with an electron beam. We have already demonstrated the use of transition radiation as an x-ray lithography source[38,56] obtaining microlithographys with circuit

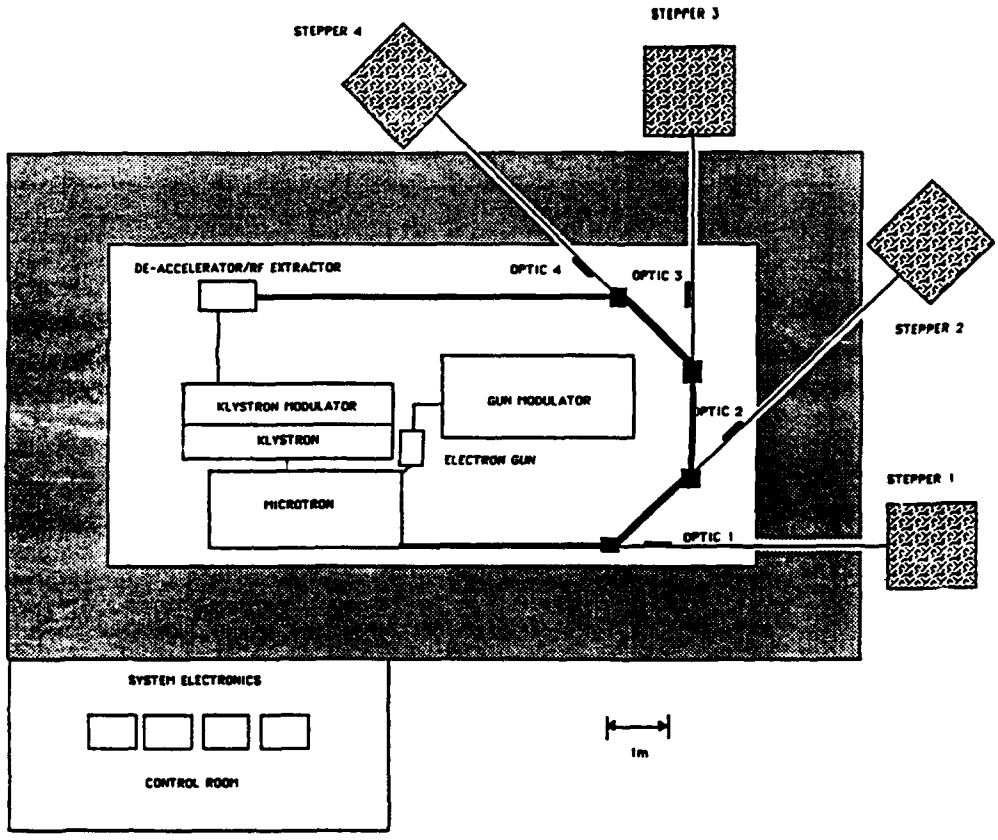

Fig. 7.1. A reduced scale drawing of a four station RTR system using a Scanditronix Microtron accelerator. The quality of the electron beam suffers little change from passage through the foils. The efficiency of the accelerator is increased by r.f. extraction from the used electron beam.

sizes of 0.5 μm and exposuring silicon wafer areas of 6 to 12 cm^2.

The efficiency of the entire x-ray system can be estimated from known accelerator, transition radiator, and optics efficiencies. Linacs can have wall-plug-to-electron-beam efficiencies of 25%. Assuming a wall plug power of 80 kW, the electron beam would be 20 kW giving approximately 30 mW of soft X-rays from the beryllium radiator. Synchrotron sources require similar power to operate in the stored-beam mode. Higher efficiencies can be obtained by recovering the electron beam microwave power after the beam has been used. The recovered rf is then reinjected into the accelerator sections for improved efficiency. This is shown in Fig. 7.1.

8. CONCLUSION

We have demonstrated that resonance transition radiation exists in the soft to warm x-ray region of the spectrum and that large number of foils can be employed to generate the x rays. In addition we have observed some bandwidth narrowing by designing foils at the photoabsorption edge of the foil material. We have experimentally demonstrated K-edge narrowing for Al, Mg, Ti, Zn, and Mo radiators. Focusing to sub-mm spot sizes has been demonstrated for both cylindrical and elliptical optics with at least a 100 fold increase in photon density over the unfocussed case. The optic permits high intensity radiation at distances larger than 3 m from the radiator. Comparison with both conventional and synchrotron sources show that such a source can be a viable alternative and perhaps fill voids in the spectrum where synchrotron sources are less available.

Our proof-of-principle experiments have demonstrated that focussed resonance transition radiation is a viable source from 100 eV to 5 keV. During phase II we would like to extend the range of the focussed source to 10 keV. We would also like to extend the demonstrate high-intensity focussed resonance transition radiation by utilizing an existing accelerator and x-ray beamline that we have already constructed. This beamline will be used to test resonance transition radiators at high average and pulsed currents. Our smoothness of the surface of our focusing optics will be improved so that the reflectivities will be sufficiently high for reflection in the 0.1 to 10 keV region of the spectrum. The resulting system will be a prototype for Phase III development.

9. REFERENCES

[1]V. L. Ginzburg and I. M. Frank, J. Phys. (USSR), **9**, 353 (1945).
[2]G. M. Garibyan, Zh. Eksp. Teor. Fiz, **33** 1403 (1958) [Sov. Phys.--JETP **6**, 1079 (1958)].
[3]M. L. Ter-Mikaelian, Nucl. Phys. **24**, 43 (1961).
[4]C. W. Fabjan and W. Struczinski, Phys. Lett., **57B**, 483 (1975).
[5]M. L. Cherry and D. Müller, Phys. Rev. Lett., **38**, 5 (1977).
[6]A. N. Chu, M. A. Piestrup, P. F. Finman, R. H. Pantell, and R. A. Gearhart, IEEE Trans. Nucl. Sci., **NS-29**, 336 (1982).
[7]P. F. Finman, M. A. Piestrup, R. H. Pantell, and R. A. Gearhart, IEEE Trans. Nucl. Sci., **NS-29**, 340 (1982).
[8]P. J. Ebert, M. J. Moran, B. A. Dahling, B. L. Berman, M. A. Piestrup, J. O. Kephart, H. Park, R. K. Klein, and R. H. Pantell, Phys. Rev. Lett., **54**, 893 (1985).
[9]M. J. Moran, B. A. Dahling, P. J. Ebert, M. A. Piestrup, B. L. Berman, and J. O. Kephart, Phys. Rev. Lett., **57**, 1223 (1986).
[10]M. A. Piestrup, D. G. Boyers, Qiang Li, M. J. Moran, F. R. Buskirk, R. M. Robinson, X. K. Maruyama, J. R. Neighbors, D. D. Snyder, IEEE Trans. on Nuc. Sci., **NS-35**, 464 (1988).
[11]M. A. Piestrup, D. G. Boyers, C. I. Pincus, Qiang Li, M. J. Moran, J. C. Bergstrom, H. S. Caplan, R. M. Silzer, D. M. Skopik, X. K. Maruyama, F. R. Buskirk, J. R. Neighbors, G. B. Rothbart, Nucl. Instrum. and Methods B **40/41**, 965 (1989).
[12]P. Goedtkindt, J. M. Salome, X. Artu, P. Dhez, M. Jablonka, N. Maene, F. Poortmans, L. Wartski, "Interference effects in x-ray transition radiation with a 500 MeV electron beam," Eleventh International Conference on the Application of Accelerators in Research and Industry, Nov. 5-8, 1990
[13]M. A. Piestrup, D. G. Boyers, C. I. Pincus, Qaing Li, G. D. Hallewell, M. J. Moran, R. M. Silzer, D. M. Skopik, X. K. Maruyama, D. D. Snyder and G. B. Rothbart, Phys. Rev. A, vol. 45, pp. 1183-1196, (1992).
[14]M. L. Cherry, G. Hartman, D. Muller, and T. A. Prince, Phys. Rev. D., **10**, 3594 (1974).
[15]A. N. Chu, M. A. Piestrup, T. W. Barbee, Jr., and R. H. Pantell, J. Appl. Phys. **51**, 1290 (1980).
[16]M. A. Piestrup, P. F. Finman, A. N. Chu, T. W. Barbee, Jr., R. H. Pantell, R. A. Gearhart, F. R. Buskirk, IEEE J. Quant. Elect. **QE-19**, 1771, (1983).
[16]G. M. Garibyan, L. A. Gerorgyan, and C. Yang, Zh. Eksp. Teor. Fiz., **66**, 552 (1974) [Sov. Phys.--JETP, **39**, 265, (1974)].
[17]M. J. Moran, Nucl. Instr. and Methods, B **33**, 18 (1988).
[18]M. A. Piestrup and M. J. Moran, Appl. Phys. Letts. **50**, 1421 (1990).
[19]M. A. Piestrup, J. O. Kephart, H. Park, R. K. Klein, R. H. Pantell P. J. Ebert, M. J. Moran, B. A. Dahling, and B. L. Berman, Phys. Rev. A, **32**, 917 (1985).
[20]M. A. Piestrup, M. J. Moran, D. G. Boyers, C. I. Pincus, J. O. Kephart, R. A. Gearhart, and X. K. Maruyama, Phys. Rev. A, **43**, 2387 (1991).
[21]M. A. Piestrup, D. G. Boyers, C. I. Pincus, J. L. Harris, R. M. Silzer, D. M. Skopik and X. K. Maruyama, Phys. Rev. A, **43**, 3653 (1991).
[22]M. A. Piestrup and P. F. Finman, IEEE J. Quant. Electr. **QE-19**, 389 (1983).
[23]M. A. Piestrup, IEEE J. Quantum Electron. **QE-24**, 591 (1988).
[24]M. B. Reid and M. A. Piestrup "The Gain of a Periodic-Dielectric-Loaded X-ray Free Electron Laser", IEEE J. of Quantum Electron. **QE-27**, 2455 (1991).
[25]Hofmann, "Theory of synchrotron Radiation" in Synchrotron Radiation Sources And Their Applications, ed. by G.N.Greaves and I.H. Munro, 1985, p.
[26]A.L. Robinson, "Synchrotron Radiation Assessed," Science, **218**,1211 (1982).
[27]S. Gruner, "Time-Resolved X-ray Diffraction of Biological Materials," Science, vol.23, p. 305, 1987.
[28]D.H. Bilderback and S. Hubbard, "X-ray Mirror Reflectivities from 3.8 to 50 keV (3.3 to 0.25 A) Part II--Pt, Si and other materials," Nuc. Instrum. and Meths., vol. 195, pp. 91-95, 1982
[29]A. Michette, Optical System for X-rays, Plenum Press, 1986.
[30]M. A. Piestrup, D. G. Boyers, C. I. Pincus, J. L. Harris, D. M. Skopik and R. M. Silzer "Lithographs

obtained from an x-ray transition radiation source," submitted Appl. Phys. Lett. (1990).
[31]K. Moffat, "Time-resolved macromolecular crystallography," Annu. Rev. Biophys. Chem. pp. 309-332 (1989).
[32]K. Moffat, "Lane diffraction: Prospects for time-resolved Macromolecular crystallography," in Strucctural Biological Applications of X-ray Absorption Scattering and Diffraction, Academic Press, p 125-133, 1986.
[32]K. Moffat, D. Szebengi, D. Bilderback, "X-ray Laue diffraction from Protein Crystals," Science Vol. 223 p 1423-1425 (1984).
[34]J. R. Helliwell, "Synchrotron x-radiation protein crystallography," instrumentation methods and applications, Pep. Prog. Phys. Vol 47 pp. 1403-1497 (1984).
[35]D. T. Attwood and K.-J. Kim, "Spectral Brightness and Coherent power of radiation from high brightness 1-6 GeV storage rings," NIM, A246 pp. 86-90 (1986).
[36]A.L. Robinson, "Synchrotron Radiation Assessed," Science, 218,1211 (1982).
[37]H. Betz, A. Heinrich, A. Heuberger, H. Huber, H. Oertel, "Resolution Limits in X-Ray Lithography Calculated by Means of XMAS," Proc. 29th Int'l. Symp. Electr., Ion, Photon Beams, Portland, Oregon, May 1985.
[38]M. A. Piestrup, M. J. Moran, B. L. Berman, P. Pianetta, D. Seligson, "Transition radiation as an X-ray source for lithography," SPIE vol. 773, Electron-Beam, X-ray, and Ion-Beam Lithographies, pp. 37-44, 1987.
[39]A. R. Robinson, "Can Synchrotron Light Save the Chip Industry," Science vol. 232, pp. 22-23, April 1986.
[40]E. Spiller and R. Feder, "X-Ray Lithography," Topics in Applied Physics, vol. 22 (ed. H. J. Queisser; Springer Verlag, Berlin, Heidelberg, New York, 1977.)
[41]A. Heuberger, "X-Ray Lithography," Solid State Technology, pp. 93-101, Feb 1986.
[42]G. F. Marshall, "Applications of Thin-Film Multilayered Structures to Figured X-ray Optics," Proc. of SPIE, 563, 114 (1985).
[42]P. Debye, "Interference of Rontgen rays and heat motions," Ann. Phys. (Leipzig), 43, 49 (1914).
[44]P. J. Mallozzi, et. al., "Laser-generated plasmas as a source of x rays for medical applications," J. Appl. Phys. 45, 1891 (1974).
[45]D. Mosher and S. J. Stephanakis, "X-ray light pipes," Appl. Phys. Lett. 29, 105 (1976).
[46]W. T. Vetterling and R. V. Pound, "Measurements on an x-ray light pipe at 5.9 and 14.4 keV," J. Opt. Soc. Am. 66, 1048 (1976).
[47]P. S. Chung and R. H. Pantell, Electron. Lett. 13, 527 (1977).
[48]R. H. Pantell and P. S. Chung, "Influence of surface roughness on the propagation of x rays through capillaries," Appl. Opt. 18, 897 (1979).
[49]A. Rindby, Nucl. Instr. and Meth. A249, 536 (1986).
[50]M. Ulmer, private communication.
[51]R. Altkorn, et.al, "Electroform replication of ultrasmooth mirrors for x-ray astronomy," Proceedings of the SPIE, Vol. 1731.
[52]R. C. Catura, E. G. Joki, D. T. Roethig, and W. J. Brookover, "Lacquer polishing of x-ray optics," Appl. Opt., 26, 1563 (1987).
[53]M. P. Ulmer, R. Haidle, R. Altkorn, P. Georgopoulos, B. Redricks, and P. Z. Takacs, "Fabrication and characterization of replicated and lacquer-coated grazing incidence optics for x-ray astronomy," Opt. Eng., 30, 1150 (1991).
[54]D. T. Attwood and K. J. Kim, "Spectral brightness and coherent power of radiation from high brightness 1-6 GeV storage rings," Nucl. Instr. and Meth. A246, 86 (1986).
[55]V.L. Highland, "Some practical remarks on multiple scattering," Nuc. Instr. and Meth. vol. 129, pp. 497-499, 1975.
[56]M. A. Piestrup, D. G. Boyers, C. I. Pincus, J. L. Harris, D. M. Skopik and R. M. Silzer "Increased x-ray power from transition-radiation source," Appl. Phys. Lett. vol. 58, pp. 2692-2694, 1991; and M. A. Piestrup, D. G. Boyers, C. I. Pincus, J. L. Harris, X. K. Maruyama, H. S. Caplan, R. M. Silzer, D. M. Skopik, "Beryllium-foil transition radiation source for x-ray lithography," Appl. Phys. Lett. vol. 59, pp. 189-191, 1991.

[57]A. N. Chu, M. A. Piestrup, T. W. Barbee Jr., and R. H. Pantell, Proc. Intl. Conf. Lasers '78, pp. 774-779, 1979.
[58]S. Datta and A. E. Kaplan "Quantum Theory of spontaneous and resonance transition radiation", Phys. Rev. A, vol. 31, pp. 790-796, 1985.
[59]Ed Graper correspondence with M. A. Piestrup, (Feb. 1991).

AFRTR.FR